A Meteorological Overview of the TC4 mission

L Pfister,[1] H. B. Selkirk,[2] D. O. Starr,[3] K. Rosenlof,[4] and P. A. Newman,[3]

L. Pfister, Earth Sciences Division, MS 245-5, NASA/Ames Research Center, Moffett Field, CA 94035-1000, USA. (Leonhard.Pfister@nasa.gov)

H. B. Selkirk, Goddard Earth Sciences and Technology Center, University of Maryland Baltimore County NASA Goddard Space Flight Center Mailstop 613.3 Greenbelt, MD 20771 USA. (Henry.B.Selkirk@nasa.gov)

D. O. Starr, NASA Goddard Space Flight Center Mailstop 613.1 Greenbelt, MD 20771 USA. (David.O.Starr@nasa.gov)

K. Rosenlof, NOAA Earth Systems Research Laboratory, Chemical Sciences Division 325 Broadway R/CSD-8 Boulder, CO 80305 USA (Karen.H.Rosenlof@nasa.gov)

P. A. Newman, NASA Goddard Space Flight Center Mailstop 613.3 Greenbelt, MD 20771 USA. (Paul.A.Newman@nasa.gov)

[1]Earth Sciences Division, NASA Ames

Abstract.

The TC4 experiment in Central America during summer 2007 was designed to address convective transport into the tropical UTLS and the evolution of anvil and in-situ formed cirrus clouds. In the Tropical Tropopause Layer (TTL), the global circulation is dominated by the Asian Anticyclone and the westward winds that stretch from the western Pacific to the Atlantic. The coldest TTL temperatures are over the Asian monsoon region, with average temperatures over Central America about 3K warmer. During TC4, TTL westward flow over Central America was stronger than normal, persisting through TC4 almost without interruption. In the upper Troposphere, the flow in the TC4 region, determined by the North American anticyclone and the Central American Convective maximum, was quite similar to climatology.

Research Center, Moffett Field, California, USA.

[2]Goddard Earth Sciences and Technology Center UMBC, Greenbelt, Maryland, USA.

[3]Laboratory for Atmospheres, NASA Goddard Space Flight Center, Greenbelt, Maryland, USA.

[4]NOAA Earth Systems Research Laboratory, Boulder, Colorado, USA.

Incidence of deep convection over the Central American region was anomalously low, being among the three lowest out of 34 years sampled. The major factor was an incipient La Nina, specifically anomalously cold temperatures off the Pacific Coast of South America. Weakness in the low level Caribbean jet caused a statistical shift in the coldest clouds from the Caribbean side of Central America to the Pacific side.

The tropopause region exhibited a rich spectrum of variability in temperature and wind. The character was largely that of upward propagating waves generated by local and nonlocal convection. These waves produced characteristic temperature variations at the cold point of 2K, with maximum peak-to-peak variation during the experiment of 8K.

At low levels in the northern portion of the TC4 region, flow from the Sahara desert predominated, while in the southern portion the air came from the Amazon region. Convectively influenced air in the upper troposphere came from Central America, the northern Amazon region, the Atlantic ITCZ, and the North American monsoon. Only a limited number of air parcels in the upper troposphere orginated from convection in the Pacific. In the tropical tropopause layer (TTL), convection to the east, including African and Asian convection, affected the observed air masses. Near San Jose and northward in the TTL, African and Asian convection (aged as much as 20 days) may have contributed as much to the air masses as Central and South American convection. South of 8N, Asian and African convection had far less impact.

1. Introduction

To address the twin science issues of upward transport into the tropical Upper Troposphere/Lower Stratosphere (UTLS) region, and the evolution of convective and in-situ formed tropical cirrus clouds, NASA conducted the Tropical Chemistry, Cloud, and Climate Coupling (TC4) field mission in Central America during the convective season. This region was selected because it was convectively active, tropical, and accessible. To understand how results in this region during the 3-week period of the experiment are globally applicable, however, we need to have a solid picture of the overall meteorological context. Specifically, we need to answer these five science questions. First, what are the basic global and regional flow patterns, and how typical are those patterns as compared to long term climatology? Second, what is the character of the convection in the region, and how does it compare to previous years? Third, how does the convection and flow vary during the three and a half week period of the experiment? Fourth, what is the nature of the dynamics of the UTLS in the TC4 region? Finally, what are the implications of the circulation for the origin of air masses sampled during the mission? The goal of this paper is to answer these five questions, and each subsequent section will address these in turn.

2. Mean tropical circulation in the boreal summer

Figure 1 shows the flow at 100mb, temperatures, positive divergence, and overall convective patterns from the average Outgoing Longwave Radiation (OLR) brightness temperatures (*Liebman and Smith* [1996]) for the extended TC4 period (July 5 - August 15), both for the year of the mission (2007) and for the 11 year average ending in 2007. 100mb is approximately at the cold point tropopause, and is thus approximately in the middle of the Tropical Tropopause Layer, or TTL (*Fueglistaler et al* [2009]). The circulation is dominated by the Asian monsoon anticyclone centered over Afghanistan, which is forced by the convection in Asia and the Bay of Bengal. It should be noted that the incidence of convective cloud tops peaks at about 13 km (150 mb); convective cloud top frequencies are down by at least a factor of 10 from this peak by the time 100mb is reached. Still, upward, cross-isentropic motion, and the divergence that forces the anticyclone (yellow contours), is maintained above the convective outflow level by momentum flux divergence from waves generated by convection (*Randel et al.* [2008]). Significant divergence in the flow field over the Asian monsoon is apparent, both in 2007 and in the 11 year average. Notably, there is no significant 100mb divergence in the TC4 region. This does not mean that convection never reaches 100mb, only that it does not have the kind of effect on the 100mb dynamics that it has in the Asian monsoon region.

Figure 1 demonstrates three points. First, the mean flow in the TC4 region (defined by the white rectangle in Figure 1), is fairly zonal and easterly (the heavy green line marks the boundary between westerly and easterly flow). This means that much of the air observed in the TC4 region at 100mb (at least for 2007) can be traced back to the region of convection over Africa and ultimately back to the Asian monsoon region. The mean 100mb easterlies slow substantially as they approach central America, which means that it takes upwards of 20 days for the air to reach Central America from the Asian monsoon region; however, during the TC4 period, the easterlies were persistent north of 5N, with only very short periods of westerly flow. In particular, after July 29, there were no periods at all of even weak westerly flow north of 5N.

Second, the coldest temperatures at this level are over Southeast Asia, with temperatures increasing steadily along the 100mb flow from east to west. In general average temperatures over Central America are about 3K warmer than over the upstream Asian monsoon. Since radiative heating is relatively weak in the summer (*Yang et al.* [2009]) this means that the air is sinking and warming and is, presumably, drier than upstream. In fact, relative humidities with respect to ice (based on MLS measurements – *Read et al.* [2007]) shown in Figure 2 indicate significantly lower values over the TC4 region than over the upstream regions of Africa and the Asian monsoon. Thus, substantial gravity and synoptic wave activity, and the lifting and temperature perturbations that accompany it, would be required for in-situ cloud formation in the TTL within the TC4 region. These clouds are almost certainly the primary mechanism by which water vapor is removed from the air that enters the stratosphere (*Jensen and Pfister* [2004]). Section 5 describes this wave activity as revealed by the local radiosondes. In fact, section 5 shows that variability generated by waves in the TTL is quite substantial, and comparable to the 3K difference in mean temperature between Central America and the Asian monsoon region.

Third, there are some significant differences between the 100mb flow in 2007 and the flow in previous years. 100mb temperatures in 2007 throughout the tropics are slightly colder than the average for the previous 11 years, partially due to the fact that QBO westerlies at 70 and 100mb are beginning to transition to easterlies (anomalously cold temperatures occur when QBO easterlies overlie QBO westerlies). Additionally, TC4 follows a significant decrease in tropical tropopause temperatures that occurred in 2001, as noted in *Randel et al.* [2006]. Also, as mentioned above, the easterlies over the TC4 region are stronger and more persistent than in a typical year, suggesting a stronger than typical link to the Asian monsoon region.

Figure 3a shows the flow at 200mb, just below the level of maximum convective outflow in the tropics. The Asian monsoon anticyclone is still a dominant global feature, but the flow west of the mid-Atlantic is much less zonal. At this altitude we see the North American anticyclone and the accompanying mid-Atlantic trough. These features essentially push the easterly flow southward. The northern part of the easterly jet over Africa is diverted northward and eastward into the mid-Atlantic, while the North American Anticyclone induces weak mean northeasterly flow over the Caribbean toward the TC4 region. Though this flow is weak, variability is substantial; thus, we expect some of the air observed at this level in the northern part of the TC4 region to have a North American origin. In contrast, the southern portion may have more influence from Asia and Africa than the air at 100mb. Another feature is the strong southwestward flow equatorward of the convective regions in Central America and the eastern Pacific. 200mb is near the level of maximum convective outflow in the tropics, and this southwestward flow is a manifestation of the strong divergence associated with Central American and northwestern South American convection (yellow contours).

At 500mb (Figure 3b), there is very little convergence or divergence and the flow is largely uniform from the east. This is consistent with the notion that, on balance, there is little net divergence or convergence associated with convection at this level. It does not mean that there is no interaction with convection at this level, merely that entrainment into convective plumes is more or less equal to detrainment from them. The significance of this flow for TC4 is that plumes from biomass burning in southern Africa, which typically ascend to midtropospheric altitudes (*Chatfield et al* [1996]) can be transported westward towards the southern portion of the TC4 region.

At 850mb (Figure 3c) flow is strongly easterly, with peak mean winds of about 10 meters per second. Convergence (yellow contours) is apparent along the convective zones extending from Africa westward through the Atlantic ITCZ, northern South America, Central America and the eastern Pacific. The slight northerly component to the easterly flow north of the convergent zone over the Atlantic implies ready advection of Sahara dust into the TC4 region, with a transit time of about 12 days. The flow is weaker within and to the west of the Central American convective region, consistent with the strong convergence associated with the convection there. South of the convergent line, the easterly flow has a southerly component. The implication here is that air from southern Africa, which is the dominant biomass burning region on the planet in July and August, can flow towards the southern part of the TC4 region. Alternatively, this air can be lofted by convection in the Atlantic ITCZ and in northern South America.

Figure 4 shows the average flow in the TC4 region during the experimental period in the boundary layer (925mb, about 700 meters above the surface) and at the bottom of the main outflow level (200mb, about 12.5 km). Sea surface temperatures form the color background in the 925mb plots, while average OLR (an indicator of cold clouds and convection) are in the 200mb plots. Turning first to the 925 mb flow, the convergence line (yellow contours) associated with the regions of low average OLR (which is in the 200mb plots, b and d) is clear. Southerly low level flow in the Pacific and a strong easterly low level jet over the western Caribbean (green contours) converge to produce strong convection in the Central American region. The low level jet exceeds 15 meters per second in an average sense, and is actually stronger than the 850mb flow. Convection and convergence on the Pacific side occur north of the strong gradient in sea surface temperatures in the Pacific. At 200mb, there is strong divergence in the wind field, from weak mean winds north of the convective region to strong northeasterly winds to the south. The magenta, cyan, and solid white contours in Figures 4b and 4d represent the 10, 20 and 25 percent contours of fraction of pixels with equivalent brightness temperatures less than 230K. Basically, these contours represent the incidences of the coldest clouds.

This figure illustrates 4 points. First, though the average OLR is similar for the TC4 period and the 11 year average, the incidence of the coldest clouds differs substantially. In the 11 year average, there is a region in the Panama Bight where over 25% of the OLR pixels have a brightness temperature less than 230K, whereas during TC4 the maximum incidence is about 20%. As will be shown in the next section, this is not just an artifact of the limited (twice-daily) temporal coverage of the OLR dataset. Secondly, though TC4 occurred during an incipient La Nina, with slightly cooler sea surface temperatures (SST) than normal, the difference in sea surface temperature in the TC4 region between the TC4 period and the 11 year average is minimal, at least in the convective region and in the Caribbean. Notably, near and just south of the equator, sea surface temperatures are significantly colder than normal. Third, overall convergence at 925mb and divergence at 200mb are quite similar during TC4 and the 11 year average. If anything, both 925mb convergence and 200mb divergence are stronger during TC4 than the 11-year average. Of note here is that comparisons of the large scale Walker circulation between the TC4 period and the 11 year average show no discernible differences. The basic conclusion is that, though the overall mass transport by convection during TC4 was similar to the average, the highest and coldest clouds, which are of substantial interest for this experiment, were less frequent than normal. Section 3 describes some of the basic character of convection in the TC4 region, how it differed statistically from the average, and why.

The fourth point regards the low level jet (green contours in the 925 mb plots), first documented by *Amador* [1998]. This is the one element of the basic circulation that *is* different, being substantially stronger during the 11 year average than during the TC4 period. Previous work (*Magana and Caetano* [2005]) shows that the strength of this low level jet is positively correlated with rainfall on the Caribbean Coast of Central America. The strengthening of this low level jet during July and August is also responsible for the well-known Mid-Summer Drought phenomenon that occurs in the Caribbean and southern Mexico (*Magana et al.* [1999]).

3. Convection during TC4

As noted in the previous section, convection during the TC4 period was, in some ways, anomalously weak. Though the overall low level convergence and upper level divergence were comparable to the 11 year average ending in 2007, the incidence of very cold cloud was significantly less than normal (Figure 4). The purpose of this section is to describe the general phenomenology of convection in this region, refine the analysis of cold cloud during TC4, and relate the observed convection to sources of long-term circulation variability in the tropics.

3.1. Diurnal Variation

Convection over land, and convection strongly influenced by land, has a strong diurnal cycle throughout the tropics. The fundamental reason is obvious – namely the land's strong response to solar heating. The average tropics typically have a peak in land convection at about 4 PM local time (based on TRMM data – *Liu and Zipser* [2008]). In tropical coastal areas, however, the diurnal cycle displays a less obvious diurnal character. *Mapes et al* [2003] have discussed the observational background and physical mechanisms responsible for the diurnal variation of convection in northwestern South America, including the Panama Bight. What follows is a brief discussion of the diurnal cycle of convection as it applies to the TC4 experiment.

Figure 5 (a-h) shows the diurnal character of convection in the TC4 region as revealed by geostationary satellite infrared imagery statistics generated over a 6 year period. What is shown is the incidence of pixels with a brightness temperature less than 210K within half degree squares from 1997-2002 for the month of July, during which most of TC4 occurred (August is very similar). We chose the 210K threshold because it more clearly differentiates those regions where convection is consistently high and cold; however, a similar picture emerges if the 230K threshold is chosen. Figure 5a shows the incidence of pixels with brightness temperatures less than 210K for 8 PM local time. This is close to the time of a broad diurnal peak in convection in northwestern South America. It is not clear why this peak is later than the tropical average for land convection (about 4 PM local time), but *Danielsen* [1982] hypothesized that it was due to cooling in the mountains and subsequent convergence in broad valleys. Convection is also quite active over other land areas, including El Salvador, southern Mexico, and the mountainous border between Costa Rica and Panama. Also apparent is the ITCZ over the Pacific, which appears as a broad enhancement in a curve from (105W, 10N) to (90W, 7N).

By 11PM local time (Figure 5b), convection over all the land areas is weaker. There is also notable movement in the convection toward the coasts and over the water. The convective complex over northwestern South America is broader, and there is enhanced cold cloud at the eastern edge of the Panama Bight. The region of convection over the Costa Rica/Panama border has split into two, with enhancements over the Caribbean and Pacific coasts. Similar behavior is seen near El Salvador. By 2 AM local time (Figure 5c) Panama Bight convection starts to develop in a major way. The convection off the Panamanian and Costa Rican coasts has moved slightly west-northwestward, and is now fully offshore. This is also the case for El Salvador. Notably, land convection over Colombia continues strongly, even though it is the middle of the night.

At 5 AM, Panama Bight convection is close to its diurnal peak, which, at least for this statistic, occurs at 6 AM. Land convection has completely subsided by this time. The Central American Caribbean and Pacific coastal convection continues to strengthen and move northwestward. The mechanisms for generating this strong coastal and Panama Bight convection, which is generally more intense than the afternoon land-based systems, is probably due to a combination of coastal convergence due to large scale flow (Figure 4) and destabilization over the oceans due to gravity waves excited by land convection the previous afternoon (*Mapes et al* [2003]). By 8 AM, Panama Bight convection is still active, but notably weaker – also the case for convection off the coast of El Salvador. In contrast, the Caribbean and Pacific coastal convection has strengthened.

The situation at 11 AM local time is shown in Figure 5f. The diurnal frequency of cold cloud is generally less than at 8 AM, not only over the Panama Bight, but over the coastal Caribbean and Pacific as well. Two developements are noted. First, the

Pacific coastal convection exhibits an apparent movement away from the shore. On an individual event basis, this exhibits itself as convective systems forming near the shore, and then traveling westward to become part of the broad ITCZ mentioned above. In fact, this clearly occurred for the systems sampled on July 17 and July 22 (*Toon et al.* [2010]). Second, there is a clear enhancement of convection off the Nicaraguan coast at this time. By 2 PM local time (Figure 5g), Panama Bight and coastal convection has nearly disappeared. Convection is now clearly developing over land areas, particularly over Panama, the eastern third of Nicaragua, the Yucatan peninsula, and Cuba. The development over land areas continues to intensify, as shown in Figure 5h. At this time, convection over Panama, the Yucatan, and Cuba is near its peak for the day. Northwestern South America is also very active, though the peak in convection in this region, as noted above, does not occur until later in the evening.

The diurnal picture outlined in Figure 5 serves a useful purpose in "classifying" the convection that was sampled during the mission. Because of the time the aircraft were in flight (typically between 6 AM and noon for the ER-2 and the WB-57, 2 PM for the DC-8), the systems that could be sampled were Panama Bight, Pacific Coastal, Caribbean coastal, and ITCZ. On one occasion (August 3) land convection over Nicaragua was sampled. During the deployment, aircraft sampled Pacific Coastal systems 5 times (7/17, 7/19, 7/22, 7/31, and 8/8), Panama Bight Systems 5 times (7/21, 7/22, 7/29, 8/3, and 8/5), and ITCZ systems 4 times (7/17, 7/19, 7/22, and 7/24). The DC-8 aircraft went near a Caribbean system on 7/22, but was flying at low altitudes under the anvils at the time. One point that should be emphasized is that diurnal variation is certainly not the whole story. Though there were very few days with no convection at all, not all the types of systems occurred on each day. Between July 14 and August 8 (26 days), Panama Bight and Caribbean Coastal convection occurred on 17 days, while Pacific Coastal convection occurred on 21 days. ITCZ convection occurred in some form (though not necessarily within range of San Jose) on each day. Most importantly, the overall strength of convection, as well as the relative strength of the systems (e.g. Panama Bight vs Pacific Coastal) varied strongly from one day to the next.

3.2. Long-term variations in convective activity

As pointed out above, the incidence of the deepest convection is significantly lower during the 2007 TC4 period than in the 11 year average. The convection in Figure 4 is based on OLR measurements, which are typically taken twice per day (*Liebman and Smith* [1996]). Given the diurnal nature of the convection and the possibility that subtle shifts in the diurnal cycle may be contributing to the anomalously low incidences of low brightness temperatures, it is appropriate to examine the same issue using a dataset with a complete diurnal cycle. Figures 6 and 7 show the incidence of brightness temperatures less than 230K and 200K respectively for all hours (based on hourly GOES-12 10.5 μm measurements) for the TC4 period (7/13-8/13) for three different years – 2005, 2006, and 2007. The basic picture is that the anomalously low convective activity for 2007 suggested by the OLR data is borne out by the GOES measurements. Turning to Figure 6, for 2005, we can see the different convective features discussed in the previous subsection, including northwestern South America, Panama Bight, Pacifc Coastal, Caribbean Coastal, and the Nicaraguan land convection occurring in the early afternoon. In Figure 6 (2005), the Caribbean Coastal convection appears as strong as the Panama Bight convection. It is clear from Figure 7, though, that the regions where the the coldest clouds occur are the

Panama Bight and northwestern South America. Notably, there is little enhancement in the frequency of brightness temperatures less than 200K over eastern Nicaraguan in 2005. The convection in that region is clearly shallower. For the most part, 2006 is similar to 2005, except with an overall reduced frequency of cold cloud over all the convective regions except for the coast of Guatemala and El Salvador (which was largely outside the TC4 operating region).

The situation is clearly different in 2007. Convection is not only less intense, but its distribution is different. Figure 6 shows that the incidence of brightness temperatures less than 230K has decreased substantially from 2006 in the Panama Bight, the Caribbean Coastal area, and over the ITCZ, (but not over the Pacific Coastal region). For brightness temperatures less than 200K (Figure 7), the area of greatest incidence is now off the coast of El Salvador. The usual enhancement in the northwestern South America/Panama/Costa Rica region that is clear in 2005 and 2006 is completely absent during the TC4 period. These figures illustrate the situation for the one month period of TC4. As shown below, deep convection in the Panama Bight was anomalously low not only for the TC4 period, but for June, and the rest of July and August as well.

Figure 8 shows the evolution through the year of convection as shown by OLR, the signed magnitude of the Caribbean Low Level Jet (*Amador* [1998]), and four measures of equatorial Pacific Ocean Sea Surface Temperature Anomalies (Nino Index Anomalies). For convection and the LLJ, both the mean annual cycle over 34 years and the behavior during the TC4 year, 2007, are shown. Mean annual values for the Nino index anomalies for any given month are all less than .4K in magnitude and are not shown. The figure illustrates three points. First, comparing the mean annual cycle in the incidence of cold

OLR cloud in the Panama Bight to 2007 (solid and dashed black lines in Figure 8a), there are clear negative anomalies from day 150 to day 260 (June 1 to the end of September). For the TC4 region as a whole (which includes the Panama Bight), the negative anomaly lasts from June until mid-August. Much of the negative anomaly for the entire TC4 region is due to the dearth of cold cloud in the Panama Bight. However, as Figures 6 and 7 show, 2007 had negative cold cloud anomalies outside the Panama Bight as well.

The second point concerns the Low Level Jet strength plotted in Figure 8b (*Amador* [1998]). Its strength is positively correlated with rainfall on the Caribbean coast (*Magana and Caetano* [2005]), and negatively correlated with rainfall in the Caribbean Sea and on the Pacific side of Central America (*Whyte et al.* [2008]). As noted by *Wang* [2007], the jet has two maxima during the year, one in mid-summer and another in January. In this figure, we plot the average zonal wind from $12 - 18°N$ and $70 - 80°W$. The broad winter maximum, and sharp summer maximum are clearly evident. During 2007, the LLJ maximum was stronger than normal in late June and early July, and weaker during the TC4 period continuing until the end of August. Clearly, anomalies in the LLJ cannot account for the overall negative anomalies in cold cloud shown in Figure 8a since there is a dearth of cold cloud in the TC4 region for the entire summer. On the other hand, the anomalously weak LLJ during the TC4 period may account for the relative strength of Pacific coastal convection as compared to the Caribbean coastal convection that is evident for 2007 in Figures 6 and 7. As noted above, increases in rainfall on the Caribbean side are related to a strong LLJ, while increases in rainfall on the Pacific are related to a weak LLJ.

The third point is illustrated Figure 8c, where four El Nino Sea Surface Temperature indices used by the NCEP Climate Prediction Center are plotted: nino12 (Coastal South America just south of the equator); nino3 (eastern equatorial Pacific); nino34 (east central equatorial Pacific); and nino4 (west central equatorial Pacific). As already noted, TC4 occurred during an incipient La Nina period, and this is clearly the case from the central and western Pacific indicators (nino34 and nino4). These two begin to develop negative deviations about the time of the TC4 experiment. For the extreme eastern Pacific, off the coast of South America, however, it is clear that temperatures were substantially colder than normal as early as May. In fact, after June 1, these are the lowest values of the nino12 index observed since 1990. The proximity of the nino12 region to the Panama Bight (which is the main source of negative cold cloud anomalies), as well as the absence of any significant correlation between Panama Bight OLR and other possible indicators (such as the Madden-Julian Oscillation – *Madden and Julian* [1971], upper level winds, and LLJ intensity) suggests this as a likely cause for the anomalously low cold cloud in the TC4 region during the experiment. Notably, the Oceanic Nino Index (a smoothed version of nino34) does have a correlation of -.5 with Panama Bight cold cloud incidence over 34 years, but cannot account for the June and July, 2007. The existence of relationships between the ENSO cycle and rainfall in Central and South America is, of course, not new (see *Amador* [2008] and *Amador et al* [2006] for reviews).

4. Meteorological Evolution during the TC4 mission

The previous sections outline important elements of the average meteorology, circulation, and convection during the mission, and how that average picture differed from a "typical" year. For a field experiment, though, shorter term variations are important.

This section will explore how these shorter term variations affected observed convection and aircraft sampling.

Figure 9 shows a summary of the evolution of the deepest convection during the TC4 period. The individual aircraft flights are shown by symbols near the top, and include some of the transit flights at the beginning and end of the mission. The two black curves are fractions of pixels in the TC4 and Bight regions (see Figure 6) that have brightness temperatures less than 225K and 200K, respectively. Essentially the solid curve depicts deep convection in the TC4 region in general, while the dotted curve focuses on the very deepest convection in the Panama Bight. The gray curve shows the minimum 700mb wind along the 77.5W meridian between 8 and 22 degrees north.

For about the first week of the mission (July 14 - July 22, julian days 195 - 203) the convection in the TC4 region was strongly modulated by three westward propagating waves (easterly waves, *Riehl* [1954]), which are depicted by the 700mb wind maximum plotted in gray in Figure 9. This led to very active convection on July 14, 15, 17, and 18, strongly suppressed conditions on July 16 and July 19, and moderately active convection on July 20-22. As shown by the figure, strong convection is roughly in phase with the easterly wind maximum at the 77.5 West meridian. The first joint ER-2/DC-8 flight took place on July 17 (day 198). Figure 10a shows the 700mb (about 3 km) winds and isotachs, along with the 6.7 μm water vapor imagery, for this date at 9 AM local time. There is strong convection off the Caribbean coast of Costa Rica, and some convection in the Panama Bight. The trough of the wave is just ahead of the strong wind enhancement associated with the wave, and is roughly at the longitude of the Nicaraguan east coast. Further east, over the Caribbean at the longitude of Venezuela, there is a dry region coinciding with the ridge of the wave. This dry region moves westward, resulting in suppressed convection on July 19 (day 200), the date of the second ER-2 flight (Figure 10b). The suppression of convection is also apparent in Figure 9, with a strong minimum in overall cold cloud in the TC4 region on day 200. The 6.7 μm features in Figure 10, which are a measure of the water vapor distribution in the 500-200mb region, show that these easterly waves have some depth, though wind perturbations above 500mb are relatively weak. Much of the time, the dry regions following the wind maxima associated with the easterly waves dissipated and moistened as they approached Central America, presumably due to convection over northern South America. In this case, however, the dry region retained its integrity. It should be noted that, though convection was suppressed in the region on July 19 compared to other days, there were still systems in the area. In fact, Pacific Coastal convection just south of Costa Rica was surveyed by the ER-2 (*Toon et al.* [2010]).

Figure 10 (bottom) does show the next easterly wave approaching, with convection over the Caribbean north of Venezuela, and a 700mb wind maximum associated with it further to the east. This wave, however, weakens substantially as it approaches Central America. By July 22, or day 203 (Figure 11a), there is significant convection in the central America region, but the dynamical signal at 700mb is weak.

As shown in Figure 9, after July 22 (day 203), there is a basic change in the character of the convection. Instead of strong pulses lasting 2-3 days with intervals of minimal convection (which is apparent from July 14-22, days 195-203), the temporal variation has a higher frequency, nearly diurnal character through August 2 (day 214, a period of almost 2 weeks). Figure 11b shows the 700mb flow for July 29, generally typical of this period.

There is evidence of an easterly wave, but it is much weaker, both in wind perturbation and in convective signature than, say, the July 17 case (Figure 10a). The absence of strong easterly surges at 700mb is also apparent in Figure 9, where easterlies never exceeded 13 m/s from days 204-214.

Though Figure 9 indicates a diurnal character to the overall level of convection in the TC4 region, there are important day-to-day variations during this period. Convection occurred in the Panama Bight region, but typically every 2-3 days (July 22, 25, 27, 30, and August 1). On other days, the strong convection would occur either north of the Panamanian and Costa Rican coasts, or south of Costa Rica on the Pacific side. In contrast to what the 11 year OLR climatology shows (Figure 4b), Panama Bight convection was not the strongest in the region during the July 23-August 2 period. The systems along the Caribbean (Figure 10a) and Pacific (Figure 10b) coasts, and in the Pacific (July 24, Figure 12 of *Toon et al.* [2010]) were actually stronger than the Bight convection. In fact, one of the deepest systems surveyed by the ER-2 and DC-8 was on the Pacific Coast just south of San Jose, occurring on July 31 (*Toon et al.* [2010], Figure 16).

This relatively quiet, quasi-diurnal period in convective activity came to an end with the arrival of a strong easterly wave on August 3 (Figure 12a). For the next 4 days (August 3-6, days 215-218), overall convective activity was substantially enhanced (Figure 9), with significant Bight convection occurring on each of these four days, most strongly on August 3. It is clear that this period of strong convection was initiated by an easterly wave, shown as a strong 700mb wind maximum in Figure 12a, accompanied by strong convection in the Caribbean. This system essentially "lit up" the whole region when it approached on August 3. Panama Bight convection exhibited the classic behavior described in Figure 4, peaking in intensity between about 9 and 12 GMT (3 to 6 AM local time). On August 4, Bight convection occurred again, though not as strongly, with the strongest convection of the day originating north of Panama and propagating northwestward.

By August 5 (Figure 12b), the 700mb wave was at the western edge of the TC4 region, but the dynamics was still quite strong, as evidenced by the region of dry air to the north and east of the TC4 region in the Caribbean. The result was continued strong convection, including in the Panama Bight (which was surveyed by all three aircraft on this date – *Toon et al.* [2010]). There followed a 2-day period of suppressed convection in the region (days 219-220, August 7-8). Bight convection was minimal on both days, so a Pacific system off the southeastern coast of Costa Rica was surveyed by all three aircraft in a coordinated mission on August 8 (Toon et al, Figure 22). As two of the aircraft departed on August 9, convective activity strengthened, with a significant system in the Panama Bight.

5. Mean structure and variability in the upper troposphere and lower stratosphere from radiosondes

High-frequency radiosonde measurements were made during the summer of 2007 by the Ticosonde/TC4 team. Sondes were released from the Juan Santamaria sonde site in Alajuela (10.0°N, 84.2°W, 883.5 m ASL) operated by the Costa Rican Instituto Meteorológico Nacional (IMN). The launch campaign ran from 00 UT June 16 through 18 UT August 15, 2007, twice daily at 00 UT and 12 UT through June 30 and subsequently four times daily. The nominal launch times were 00, 06, 12 and 18 UT, but these were occasionally adjusted to enable coincidence with satellite overpasses. The radiosonde used was the Vaisala RS-92SGP radiosonde equipped for GPS windfinding launched on both

500-g balloons filled with hydrogen and 600-g balloons filled with helium. Sondes were launched under the supervision of IMN staff with the assistance of a student team from the Universidad de Costa Rica. A total of 197 radiosondes were released over the 61 days of the campaign. Of these 179 reached at least 20 km before termination, normally due to balloon burst. The ascent reached a median altitude of 32.1 km, and the highest reached 34.365 km (6.1 hPa).

The IMN maintains a Vaisala MW11 ground station at the sonde site; this was upgraded for our Ticosonde campaign in 2005 (*Vömel et al.* [2007]; *Selkirk et al.* [2010]) for reception of the digital signal from the RS92. The MW11 provided data every 2 seconds for ascent rate, pressure, altitude, temperature, relative humidity, dewpoint, wind direction and wind speed. At the campaign mean ascent rate of $5.27 m/s$, this is nearly equivalent to logging data every 10 meters, and so we interpolated our data to a 10 meter grid for the analysis here.

These radiosonde measurements allow us to characterize the mean temperature structure in the Upper Troposphere/Lower Stratosphere (UTLS) region, as well as its variability. Coupled with the winds, the mechanisms (for example, the types of wave motions) for generating this variability can be understood. In the context of this experiment, designed to look at clouds and tracer transport in the UTLS, the variability and persistence of cold temperatures is a key driver for cloud maintenance and generation. In fact, since Central America is *not* the coldest region in the TTL at this time of year, temperature variability is *the* most important variable in understanding the formation of the TTL clouds that dehydrate air that enters the stratosphere.

5.1. Mean Structure

Figure 13 is a Stuve diagram with the average profiles of temperature and dewpoint along with barbs of the mean winds. The temperature profile in the upper troposphere is roughly moist adiabatic up to $\sim 12km$, and there is a pronounced stabilization above 150 hPa where the lapse rate decreases to $< 2°C/km$ in the layer immediately below the profile minimum temperature at 96 hPa. Also shown in the figure are the individual cold point tropopauses which form a cluster ranging down to this stabilization level and upward to nearly 70 hPa. The average of the cold point temperatures from all the soundings before gridding was $-78.8 \pm 1.4°C$ and was located at $379.7 \pm 13K$ potential temperature and $16.81 \pm .71km$ altitude. Cold point potential temperatures ranged from 352 K to 418 K; the coldest cold point was $-83.8°C$ and was observed at 368.7 K and 16.74 km. The mean cold point saturation mixing ratio was 4.4 ± 1.1 ppmv and the saturation mixing ratio of the minimum cold point was 1.86 ppmv, though this is an outlier over two standard deviations below the mean. Despite the strong diurnal variation in convection, both locally and regionally, there was no statistically significant diurnal variability at Alajuela in any of the cold point variables mentioned above, although at 06 UT the cold point tropopauses were $\sim$ 200 m higher than the diurnal average and a few degrees higher in potential temperature.

Figure 14a shows the profiles of the standard deviation of temperature and dewpoint. The temperature profile above the boundary layer is fairly constant at $\sim$ 1°C, but at 13.66 km and 350 K there begins a sharp variability gradient. The variability then settles down to a level of $\sim 2°C$ which prevails from $\sim$ 15 km up to the middle stratosphere where it ramps up to $\sim$ 3°C up to the limit of our data at 35 km. We will show below that the rapid increase of variability above 350 K is in large part a consequence of a rich spectrum of wave energy from inertial to synoptic and longer timescales in the TTL that propagates up through the stratosphere.

The vertical structure of dewpoint variability is rather different. The standard deviation peaks between 5 and 11 km and then decreases to a relative minimum of $< 3°C$ at 15 km. This decrease is probably due to the decreasing sensitivity of the humicap sensor pair in the Vaisala RS92.

Figure 14b shows the profiles of the zonal and meridional wind bracketed by envelopes of ± 1 standard deviation. Winds are east-southeasterly above the boundary layer, then become easterly and then east-northeasterly above 10 km. Above this level the variability in both components begins to increase noticeably; the standard deviation of zonal wind has more than doubled at its easterly maximum of $> 7.7 m/s$ near 13 km, and there is an even greater increase for the meridional component up to 15 km. At 15.75 km the meridional component vanishes, and the zonal component is also close to its minimum value of $-3.35 m/s$ for the whole profile above the boundary layer. Above this level there is a steady mean easterly gradient up to 28 km, while the magnitude of the mean meridional wind remains $\leq 1 m/s$. The peak easterly wind of $\sim 38 m/s$ prevails in a layer about 1.5 km thick above 28 km, above which there is a decline to $\sim 25 m/s$ above 30 km.

5.2. Variability

Figure 15 shows the time series of cold point tropopause temperature from the radiosondes at Alajuela over the period of the Ticosonde/TC4 campaign. The figure shows the observations as well as a binomially smoothed (N=51) version of the time series interpolated from the observations using cubic splines. The figure shows a high degree of short-term variability, but the filtered time series emphasizes the variations on longer, multi-day time scales. Variability at or near the local inertial period of 2.88 days is apparent, as are longer period synoptic scale variations, including variability on time scales of 2-3 weeks, particularly towards the end of the record (days 205-226).

Figure 16 shows time-height cross-sections of temperature, zonal wind and meridional wind anomalies. These cross-sections were constructed from time series of anomalies at each of the 10-m grid levels. In addition to removing the time mean at each level, each time series was also adjusted to remove any small temporal trend. For the purposes of these plots, the anomaly time series at each level were interpolated in time; we set the maximum height for the plots in the figure as that altitude where gaps of no more than 6 points were observed in any of the three variables. After the interpolation, each time series was also smoothed with a 5-pt boxcar (running mean average) filter to remove any strong diurnal variability.

The vertical structure of the variability of temperature and winds shown by Figure 14 is evident in the cross-sections in Figure 16, *viz*, the gradients above 13.5 km in temperature and above 10 km in the winds. In the 10-16 km layer, the wind variability is dominated by meridional wind anomalies with a period of approximately 8 days. This is confirmed by the spectral analysis results shown in Figure 17. They show a prominent peak centered at this period between 10 and 16 km and secondary and much weaker peak right at 15 km at the local inertial period of 2.88 days. In contrast, upper tropospheric variability in the zonal wind is less well organized and at longer time scales.

The character of the anomalies undergoes a marked change above 15 km. From here up to 25 km, the temperature anomalies become prominent and show a downward phase propagation that is remarkably coherent at times. Figure 17a shows that in the 17-20 km region, i.e. the layer immediately above the cold point tropopause, there is a peak of temperature variability with periods of $\sim$ 4 days and longer, while there is a relative minimum in variability between 20 and 22 km. Above this level there is increasing spectral power centered at periods of 4 days and between 8 and 16 days. In contrast, spectral power in both the meridional and zonal winds falls off strongly above the cold point tropopause, and there is a relative minimum of wind power in a layer several kilometers deep above 20 km. Above 25 km there emerges broad peak of energy in the zonal wind centered at a period of 8-10 days, which grows into a very strong peak at these frequencies above the layer of maximum easterly winds (Figure 14b). At this level and range of frequencies, there is only a weak peak in meridional winds; however, both wind components display strong peaks at the inertial period above 31 km. Finally, at 17 km (the approximate altitude of the cold point tropopause – Figure 13) there is a shallow (vertically) peak in temperature power covering periods from 1.7 to 3 days.

The change from vertical coherence of the wind anomalies below 15 km to a pattern of downward phase propagation and upward energy propagation in all variables suggests that the regional atmosphere, and in particular the temperature at the tropopause, is responding to deep convective forcing. In a near-equatorial region, the response in the stratosphere can include both eastward-moving Kelvin waves and westward-moving mixed Rossby-gravity or Yanai waves and equatorial Rossby waves (see *Wheeler et al* [2000]). The easterly wind in the stratosphere prevents propagation of westward-moving modes so it is to be expected that the limited meridional wind spectral power at the inertial frequency is due to local inertial instability. On the other hand, cross-spectral analysis of

T, u and v (not shown) shows a peak in the cospectrum of T and v near 15 km centered between 8 and 16 days. This may well be the signature of mixed Rossby-gravity waves strongly evanescent in height. Likewise at these upper tropospheric levels, the cospectrum of u and v has a peak in the same frequency range, also evidence of mixed Rossby-gravity waves. In contrast T and u show only a weak relationship. Thus the dominant synoptic-scale response to convective forcing appears to be in the mixed Rossby-gravity modes and not in Kelvin modes.

6. Origin of air masses sampled during TC4

The mean circulation and convection described in Sections 2 and 3 respectively have implications for the air masses sampled during the TC4 mission. Given meteorological variance, however, any complete discussion of air mass origins requires a full trajectory treatment. In this section, we use kinematic and diabatic trajectory analysis to develop a climatology of the origins of air parcels that are observed within the time and region of aircraft operations. Specifically, we will answer three questions: (1) what is the origin of the air at low levels, specifically 850mb (about 1.6 km, just above the boundary layer)?; (2) what is the origin of the air in the upper troposphere near the main tropical convective outflow level at 200mb, and where is the convection that feeds that air?; and (3) what is the extent of convective influence in the Central American TTL (about 100mb), and which convective systems are responsible?

The approach is to establish a 1 by 1 degree grid of points in the TC4 region, from 5S to 20N and 90W to 75W at each of the three relevant altitudes (850mb, 200mb, and 100mb), and calculate trajectories on 13 separate days during the experiment using a kinematic formulation for 200mb and 850mb, and a diabatic formulation for 100mb (*Schoeberl and*

Sparling [1995]). The 13 days are spaced evenly through the experimental period (July 17 through August 10), so we perform a trajectory analysis every other day. Thus, for each altitude, 5408 trajectories are calculated. The kinematic formulation uses three-dimensional winds based on 6-hourly analyses (on a 1 by 1 degree grid) from the Global Data Assimilation System(GDAS) of the National Center for Environmental Prediction (NCEP). At 100mb, diabatic trajectories are used because the vertical winds are less reliable. In this formulation, trajectories are calculated isentropically, with movement upward and downward through the isentropes governed by clear sky heating rates.

6.1. Lower and Upper Troposphere Air origin

Figure 18 (a-d) shows the results for 14-day back trajectories originating at 850mb in the TC4 region. The accuracy of trajectory calculations varies with the meteorological situation, with a typical rule of thumb suggesting that results begin to diverge at about a week. For a climatological study, however, where one is not trying to trace the origin of a particular air mass, longer integrations will yield useful information. We choose 14 days partly for practical reasons, but also because we expect parcels to lose their integrity due to mixing processes in about 2 weeks. Each trajectory is represented by 701 points (one every half hour), and we use the locations of every fourth point along each trajectory to develop the plotted distributions. The figures are essentially geographically distributed percentage distribution functions, where the color in each geographical rectangle (sized 10 degrees latitude by 10 degrees longitude) represents the percentage of all points along all relevant 14 day trajectories that are to be found in that rectangle. The four separate figures (a-d) represent distributions for back trajectories originating in four quadrants of the TC4 region as indicated in the figure caption.

Figure 18a and 18b show distributions for parcels originating in the northwestern and northeastern quadrants of TC4 operations, respectively. Perhaps the most remarkable feature is the "channel of air origin" heading eastward towards North Africa, and the almost complete absence of any points west of the TC4 region. This is an indication of the strength and persistence of the low-level easterly flow depicted in Figure 3c. Nevertheless, there is some dispersion in the parcel distributions. Some parcels have spent a significant amount of time over the northern Amazon region (Venezuela and the Guianas). Had the trajectories been extended for another week, one might see some parcels traced back to the biomass burning region in southern Africa. For the northwestern quadrant (Figure 18a), a small number of parcels can be traced back to the southern hemisphere westerlies.

Results are substantially different for the two southern quadrants (southwestern – Figure 18c; southeastern – Figure 18d). Though there is still evidence of a "channel" toward the Sahara desert, the distribution around the TC4 region is more symmetric. At these latitudes, much of the air at low levels comes from the Amazon. Also, there is a larger contribution from the southern midlatitudes, as air occasionally moves north along the Pacific coast just west of the Andes.

Figure 19 (a-d) shows the results for 14-day back trajectories originating at 200mb. Unlike Figure 18, where the distribution of all points are plotted, we plot only the points above 300mb. This separation is done since 200mb is just below the main outflow level in the tropics. The goal is to see from where air parcels that do *not* undergo convective lifting come. In this calculation, about half of all the points along the trajectories are above 300mb, and this does include points on trajectories that dip below 300mb and rise back up again. Turning to Figures 19a and 19b, we see a much broader directional distribution than at 850mb. This arises from the fact that there are two main pathways to these two regions as suggested by Figure 3a; one pathway is from North America around the anticyclone and upstream of the mid-Atlantic trough, and the other is from the east and the southern edge of the Asian anticyclone. These two pathways are reflected as two angular maxima in the distribution, one pointing eastward and the other pointing north-northeastward. Note that though it takes longer than 14 days for air to go from the Asian anticyclone to Central America, air movement along the northern hemisphere westerlies and around the anticyclone is fairly rapid. A small number of parcels have actually traveled all the way from central Russia eastward, across the Pacific, and equatorward to Central America.

The distribution of air parcels ending in the southern portion of the TC4 region has a different character (Figure 19, c and d). Here, there is a significant contribution of parcels from the Pacific ocean. This is an apparent inconsistency with the mean flow pattern in Figure 3a. In fact, at about the turn of the month (July 30 through August 2, just prior to the strong convective events of August 3, day 215, Figure 9), strong 200mb westerly winds penetrated to about 3N. This was an unusual event. The fact that there is no convection in the eastern Pacific just south of the equator means that this event will have a disproportionate impact on the statistics for parcels remaining at high altitudes, since, as shown in the discussion of Figure 20 below, about half the parcels experience significant convective uplift. The other sources of air for the southern part of the TC4 region are similar to those for the northern part, namely the easterly jet emanating from the Asian monsoon anticyclone, and the north American monsoon anticyclone. As expected, the latter is not as prominent as in Figures 19a and 19b.

Figure 19 showed the geographical distribution of trajectory points above 300mb from parcels originating at 200mb. Figure 20 (a-d) shows the distribution of positions of those parcels that ascend to 200mb from below 700mb via the resolved wind fields at some time during the previous 14 days, and the locations where the ascent occurred (specifically where the parcels crossed the 500mb surface – yellow dots). As indicated in the figure, a bit less than half of the parcels in all four quadrants have ascended. Given the difficulty of projecting convective effects onto a 1 by 1 analysis grid, this exact number should not be treated too seriously. A similar uncertainty would apply to equating the exact locations of the 500mb crossing to the location of convection, since the trajectory calculation is likely to produce a much gentler slope in the ascent than is actually occurring in convective systems. Given the easterly flow that predominates at all the altitudes (Figure 3), this means that the 500mb crossing point is probably somewhat east of the actual convection.

Still, the analysis provides some indication of where the ascent occurs, and where low level parcels ending up in the Central American Upper Troposphere might originate. In all four quadrants, ascent in the Atlantic ITCZ, northern South America, and the Caribbean are important in lofting air to 200mb from low levels. In all except the northwestern quadrant (Figure 20a), some ascent occurs over Africa. Ascent over the eastern Caribbean plays an important role for the northeastern quadrant (Figure 20b). One interesting pathway for air is apparent in the two northern quadrants (Figure 20a and b). Here air from low levels in North America is lofted by North American convection and transported southward to Central America. However, in all cases, most of the air that has ascended comes from a broad swath that is east of Central America. The basic picture is one of air converging from north and south of the ITCZ in the Atlantic and equatorial South

America, and ascending over the Atlantic, South America, the Caribbean, and Central America.

6.2. TTL Air origin

Figure 21 (a-d) shows the results for 14-day back trajectories originating at 100mb. 100mb is essentially in the middle of the TTL, and, in Central America, is very close to the cold point tropopause (Figure 13). Only the distribution of parcel positions above 200mb is shown, though it turns out that parcels in this kinematic trajectory formulation stayed above 200mb about 97% of the time. As in Figure 19, the two northern and two southern quadrants show similar characteristics. Parcels originating in the two northern quadrants (Figures 21 a and b) have a strong "channel of origin" pointing eastward, consistent with the global influence of the Asian monsoon easterly jet shown in Figure 1. In a few cases, it only takes 14 days to go from the monsoon region to Central America; in fact, there is evidence that parcels could come from as far away as Japan in this time. Unlike 200mb, influence from air in North America is very limited. The situation for the two southern quadrants is quite different. Though a significant number of parcels come from the east, others come from the west. A significant number of parcels have actually gone eastward from South Africa across the Indian and Pacific oceans and ended up in Central America within 14 days. Again, this is entirely consistent with Figure 1, which shows mean westerly winds south of about 5N.

The kinematic trajectory formulation using the NCEP analyses is not likely to give a good indication of the influence of convection at the 100mb level, if only because 100mb represents the top level of the available vertical wind grid for the particular analysis product used (though not the top level for other meteorological variables). Thus, to get some indication of convective influence in the TTL, we use a different approach. Figure 22 (a-d) shows the results of a convective influence analysis based on a combination of diabatic trajectory analysis and global geostationary infrared imagery. The method, similar to that documented in *Pfister et al.* [2001], starts with a set of back trajectories originating in the TC4 region. Back trajectories are started at the same dates and times as for the kinematic approach, except that vertical motions are calculated by forcing parcels to follow isentropes, with a correction using average summer clear-sky radiative heating rates. The calculations are done for 20 days instead of 14, the justification for this being that mixing rates are probably less at 100mb than at 200mb, thus allowing parcels to retain some integrity for a longer time. As mentioned above, though the accuracy of individual trajectories is poor beyond a week, there should be some statistical validity to large groups of trajectories.

To evaluate the impact of convection, the trajectories are marched through a time varying field of global geostationary infrared (10.5 μm) imagery. Convective interaction occurs if the cloud altitude (based on brightness temperature) matches the altitude of the trajectory. *Sherwood et al* [2004] and *Minnis et al* [2008] have noted that cloud altitudes from IR methods are typically about 1 km below actual altitudes based on lidar altimetry. This applies even for optically dense clouds, such as convective anvils. Thus, brightness temperatures are adjusted by 6K (consistent with the typical lapse rate in the TTL) before convective interaction is evaluated. To account for the thinning of anvils at their edges, parcels must only come within 30km of a given pixel to allow interaction. Effectively, at any given time, the parcel is said to be influenced by the coldest pixel within 30km, a number based on crude observations of the size of anvil edges. It should be emphasized that this method tells us if a parcel has come within 30km of a cloud with an altitude that is at least as high as the parcel. It is thus an indicator of whether a parcel has been influenced by convection. The method cannot tell us what fraction of the air is from the convective plume, and what fraction is from the environment.

The results are shown in Figure 22 (a-d). What is plotted are the locations where individual parcels experience their most recent convective encounter, color coded for the elapsed time between convective interaction and arrival in the TC4 region. The percentages on the figure indicate the overall fractions of parcels in each quadrant that is influenced by convection in particular regions. The first thing to note is that the overall proportion of air influenced by convection (average of about 65% for all four quadrants) is larger than the values deduced for the main outflow layer at 200mb (Figure 20). In fact, the implied convective turnover time (65% of the air in 20 days) is about half the tropical average turnover time (60 days) calculated by Dessler (2002) at 375K (the approximate potential temperature at 100mb). To put these discrepancies into context, we note three things. First, this calculation attempts to establish convective *influence*, rather than complete turnover of a given air mass. It is thus not really calculating the same quantity as shown in Figure 20 (which may, in fact, be an underestimate). Convective anvils are mixtures of convective and environmental air, and air near the anvil tops (which is the situation here, since only the deepest systems reach 100mb – *Gettelman et al.* [2002]) is likely to have a large admixture of environmental air. Third, we might well expect a faster than average tropical convective turnover time for a region that is not only convectively active but is directly downstream of other convectively active regions. Finally, this technique, just like any technique that attempts to quantify the effect of convection, is imperfect and includes assumptions (e.g., the 30 km "influence region" indicated above) that will affect the results. Thus, errors are expected, though our expectation is that they are perhaps a factor of two, rather than a factor of ten.

In spite of the expected errors, the approach has value, especially for looking at water vapor and water vapor isotopes (*Sayres, et al.* [2010]), where nearly any contact with a convective system at high altitude is likely to saturate the air. Also, it has the advantage of being based on actual observations of convection rather than convective parameterizations.

The results for the two northern quadrants (Figures 22a and b) show that convection lining up along a "highway" from the east is influencing the air in the northern part of the TC4 region. There is a small contribution from North American convection (defined as western Hemisphere north of 20N), but, in general, convection in the zones outlined by the OLR minima in Figure 1 (Tropical Americas, Africa, and Asian monsoon) are the major contributors. Note that it typically takes about 15 to 20 days for air to travel from the Asian monsoon region to Central America. Travel times are 10-16 days for African convection. Of particular note is that the Atlantic ITCZ, which is so important at 200mb, plays very little role at 100mb. The picture in the southern two quadrants (Figures 22c and d) is similar, but with some important differences. Though "nearby" convection (essentially western hemisphere south of 20N) contributes about the same amount, the contributions from African and Asian convection are much smaller, consistent with the greater spread of trajectory origins (Figures 21 c and d) and the position of the zero time-mean zonal wind line (Figure 1a). Another notable difference from the northern quadrants is a contribution from the convective zone south of Mexico to the west of the TC4 region. This convective zone appears as as a secondary minimum in OLR in Figure

1a. On a number of occasions (e.g., *Petropavlovskikh et al.* [2010]), northerly flow from this convective zone curved eastward into the southern portion of the TC4 region. This is also why there is actually a greater contribution from Mexican convection in the southern quadrants than in the northern quadrants. Easterly flow was much more persistent into the northern quadrants, severely limiting any influence from convection to the west.

7. Summary and Conclusions

The purpose of this overview has been to set the meteorological context for the TC4 aircraft experiment, whose purpose was to research the processes of convective transport in the UTLS and cirrus cloud evolution in the tropics. Intensive aircraft campaigns, by their very nature, focus on a limited region in a limited time. The advantage is that important details of microphysical and transport processes that cannot be elucidated by global satellite measurements, either because of inadequate spatial resolution or that the quantity simply cannot be measured, can be addressed. The disadvantage is that conditions in the sampling time and region may not be typical, and deviations from the average need to be understood. For example, microphysical processes in cirrus clouds are strongly affected by temperature, a quantity subject to variations on all scales, from near microscale gravity waves to interannual variations. Furthermore, convective transport occurs in many locations on the globe. Evaluating it thus requires an understanding of the lateral transport of air masses.

At the highest levels of interest, namely the Tropical Tropopause Layer, the global circulation is dominated by the Asian Anticyclone and associated easterly winds. These winds originated in generally colder regions to the east, and, not surprisingly, relative humidities in the TC4 TTL are generally lower than most regions upstream. Temperatures were colder than normal, consistent with the tropopause temperature drop in the tropics noted earlier in the decade. The lower relative humidities in the TC4 region mean that in-situ cirrus formation in the TTL is particularly dependent on having significant deviations from the mean temperature. The radiosonde observations showed very substantial variability in temperature and wind, largely displaying the character of upward propagating waves generated by convection in the region. These waves produced characteristic temperature variations at the altitude of minimum temperature on the order of 2K, with a maximum peak-to-peak variation of 8K exhibited during the experiment.

In the upper and middle troposphere, flow is also easterly, but there is no obvious deviation from typical conditions at these levels. Overall convective divergence at the maximum tropical outflow level (about 200mb to 150mb) is similar to average conditions for the time of year in which the experiment was conducted. This is not inconsistent with expectations from the state of the ENSO cycle, which was nearly neutral, but in the early stages of La Nina conditions.

The central American region is the primary region of convective convergence at low levels in the Tropical Western Hemisphere, and the overall magnitude of this convergence was similar to climatological conditions. Important difference were in the strength of the low level Caribbean jet (which was weaker than normal), and the colder than normal sea surface temperatures off the equatorial coast of South America.

This may have had implications for the overall incidence of the deepest convection during the three week period of the experiment. Here, the TC4 period showed the largest deviation from normal conditions, with the coldest clouds showing the third lowest incidence in 34 years of Outgoing Longwave Radiation statistics. A comparison of geostationary satellite statistics for three years showed that the largest deviation was in the Panama Bight region, with negative deviations of 30% or more from the same period in 2005. Most of this deviation can be attributed to the incipient La Nina conditions, particularly the anomalously cold temperatures off the equatorial coast of South America. The effect of the relative weakness of the low level jet was on the overall distribution of convection in the TC4 region. Consistent with previous studies, the effect was to strengthen Pacific coastal convection relative to Caribbean coastal convection.

Convection and the overall circulation determine the nature of the observed air masses. At low levels in the northern portion of the TC4 region flow from the east-northeast predominated, while flow from the Amazon predominated in the southern portion. In the upper troposphere convectively influenced air came from Central America, the northern Amazon region, the Atlantic ITCZ, and the North American monsoon. Only a limited number of air parcels in the upper troposphere orginated from convection in the Pacific. In the TTL, convection to the east, including African and Asian convection, affected the observed air masses. Near San Jose and northward in the TTL, African and Asian convection (aged as much as 20 days) may have contributed as much to the air masses as Central and South American convection. South of 8N, Asian and African convection had far less impact.

Acknowledgments. The authors of this paper would like to acknowledge support from the NASA Upper Atmosphere Research Program, the NASA Atmospheric Chemistry Modeling and Analysis Program, and the NOAA Atmospheric Composition and Climate program.

References

Amador, J. (2008), The Intra-Americas Seas Low-Level Jet (IALLJ): Overview and Future Research. *Annals of the New York Academy of Sciences, Trends and Directions in Climate Research*, L. Gimeno et al, editors, *1146*, 153-188.

Amador, J., E. J. Alfaro, O. G. Lizano, and V. O. Magana (2006), Atmospheric forcing of the eastern tropical Pacific: A review. *Progress in Oceanography, 69*, 101-142.

Amador, J. (1998), A climatic feature of the tropical Americas: the trade wind easterly jet, *Top. Meteor. y Ocean., 5*, 91-102.

Chatfield, R., J. Vastano, H. Singh, and G. Sachse (1996), A general model of how fire emissions and chemistry produce African and oceanic plumes (O3, CO, PAN, smoke) in TRACE A, *J. Geophys. Res., 101*, 24279-24306.

Danielsen, E. (2009), Statistics of Cold Cumulonimbus Anvils Based on Enhanced Infrared Photographs, *Geophys. Res. Ltrs., 9*,601-604.

Fueglistaler, S., A. E. Dessler, T. J. Dunkerton, I. Folkins, Q. FU, and P. W. Mote (2009), Tropical Tropopause Layer,*Revs Geophys., 47*,doi:10.1029/2008RG000267.

Gettelman, A., M. L. Salby, and F. Sassi (2002), Distribution and influence of convection in the tropical tropopause region, *J. Geophys. Res., 107*, ACL6-1-6-14.

Jensen, E. J. and L. Pfister (2004), Transport and Freeze-drying in the Tropical Tropopause Layer, *J. Geophys. Res., 109*, doi:10.1029/2003JD004022.

Liebmann, B. and C. A. Smith (1996), Description of a complete (interpolated) Outgoing Longwave Radiation Dataset. *Bull. Amer. Met. Soc., 77*, 1275-1277

Liu, C, and E. J. Zipser. (2008), Diurnal Cycles of Precipitation, Clouds, and Lightning in the Tropics from 9 Years of TRMM Observations, *Geophys. Res. Ltrs., 35*, doi:10.1029/2007GL032437.

Madden, R. and P. Julian. (1971), Detection of a 40-50 day oscillation in the zonal wind in the tropical Pacific, J. Atm. Sci., *28*, 702-708.

Magana, V. and E. Caetano, (2005), Temporal Evolution of Summer Convective Activity over the Americas Warm Pools, *Geophys. Res. Ltrs., 32*, doi:10.1029/2004GL021033.

Magana, V., J. A. Amador, and S. Medina (1999), The Midsummer Drought over Mexico and Central America, *J. Clim., 12*, 1577-1588.

Maloney, E. D., and J. T. Kiehl (2002), MJO-Related SST variations over the Tropical Eastern Pacific during Northern Hemisphere Summer, *J. CLim, 15*, 675-689.

Mapes, B. E., T. T. Warner, M. Xu, and A. J. Negri (2003), Diurnal Patterns of Rainfall in Northwestern South America. Part I: Observations and Context, *Mon. Weath. Rev., 131*, 799-812.

Mapes, B. E., T. T. Warner, and M. Xu (2003), Diurnal Patterns of Rainfall in Northwestern South America. Part III: Diurnal Gravity Waves and Convection Offshore, *Mon. Weath. Rev., 131*, 830-844.

Minnis P., C. R. Yost, S. Sun-Mack, Y. Chen (2008), Estimating the top altitude of optically thick ice clouds from thermal infrared satellite observations using CALIPSO data, *Geophys. Res. Lett., 35*, L12801, doi:10.1029/2008GL033947.

Pena, J. and M. W. Douglas (2002), Characteristics of Wet and Dry Spells over the Pacific Side of Central America during the Rainy Season, *Mon. Weath. Rev., 130*, 3054-3073.

Petropavlovskikh, I. *e*t al. (2010), Low ozone bubbles observed in the TTL during the TC4 campaign in 2007, *J. Geophys. Res.,* This special issue.

Pfister, L., *e*t al.(2001), Aircraft Observations of Thin Cirrus Clouds near the Tropical Tropopause, *J. Gophys. Res., 106*, 9765-9786.

Randel, W. J., R. Garcia, and F. Wu, (2008), Dynamical Balances and Tropical Stratospheric Upwelling, *J. Atmo. Sci., 65*, 3584-3595.

Randel, W. J., F. Wu, H. Vömel, G. E. Nedoluha, and Pl Forster (2006), Decreases in stratospheric water vapor after 2001: Links to changes in the tropical tropopause and the Brewer-Dobson circulation, *J. Geophys. Res., 111*, D12312, doi:10.1029/2005JD006744.

Read, W. G. et al (2007), Aura Microwave Limb Sounder upper tropospheric and lower stratospheric water and relative humidity with respect to ice validation, *J. Geophys. Res.,*,D24S35, doi:10.1029/2007JD008752.

Riehl, H. (1954), *Tropical Meteorology*, McGraw-Hill, 392pp.

Sayres, D. S. *e*t al. (2010), The influence of convection on the water isotopic composition of the TTL and the tropical stratosphere, *J. Geophys. Res.,* This special issue.

Schoeberl, M., and L. C. Sparling, Trajectory modelling, diagnostic tools in atmospheric science,(1995) *Proc. Int. School of Phys.*, 289-305.

Selkirk, H. B., H. Vömel, J. Valverde, and L. Pfister (2010), The detailed structure of the tropical upper troposphere as revealed by balloonsonde observations of water vapor, ozone, temperature and winds during the NASA TCSP and TC4 campaigns, *J. Geophys. Res.,* This special issue.

Sherwood S. C., J.-H. Chae, P. Minnis, M. McGill (2004), Underestimation of deep convective cloud tops by thermal imagery, *Geophys. Res. Lett., 31*, L11102, doi:10.1029/2004GL019699.

Toon, O. B. et al. (2010), Planning and implementation of the Tropical Composition, Cloud, and Climate Coupling Experiment, *J. Geophys. Res.,* This special issue.

Vömel, H., H. Selkirk, L. Miloshevich, J. Valverde, J. Valdes, E. Kyro, R. Kivi, W. Stolz, G. Peng, and J. A Diaz (2007), Radiation dry bias of the Vaisala RS92 humidity sensor, *J. Atm. Oc. Tech.*,*24*, 953-963.

Wang, C. (2007), Variability of the Caribbean low level jet and its relations to Climate, *Climate Dynamics, 29*, 411-422.

Wheeler, M., G. N. Kiladis, and P. J. Webster,(2000), Large-scale dynamical fields associated with convectively coupled equatorial waves. *J. Atm. Sci., 57*, 613-640.

Whyte, F. S., M. A. Taylor, T. S. Stephenson, and J. D. Campbell (2008), Features of the Caribbean low level jet, *International Journal of Climatology, 28*, 119-128.

Yang, Q., Q. Fu, and Y. Hu (2009), Radiative impacts of clouds in the tropical tropopause layer, *J. Geophys. Res.,* submitted.

Yang, G-Y, and J. Slingo (2001), The Diurnal Cycle in the Tropics, *Mon. Weath. Rev., 129*, 784-801.

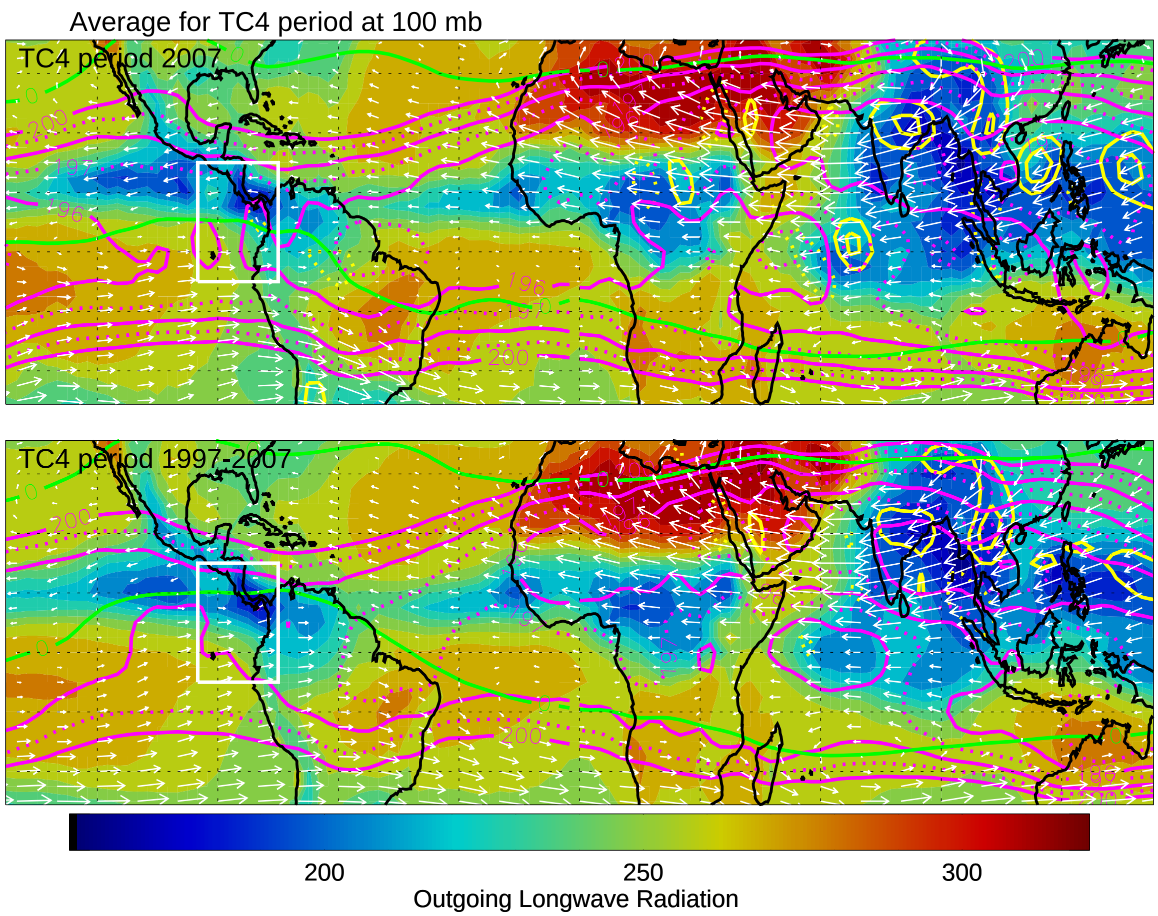

Figure 1. Average meteorology at 100mb for the extended TC4 period (July 5-August 15) for 2007 (the year of the mission) and for the 11 year average 1997-2007. Color fill: OLR; magenta contours: temperature; yellow contours; positive divergence; green contours: zero zonal wind line. The white rectangle denotes the approximate limits of TC4 flight operations.

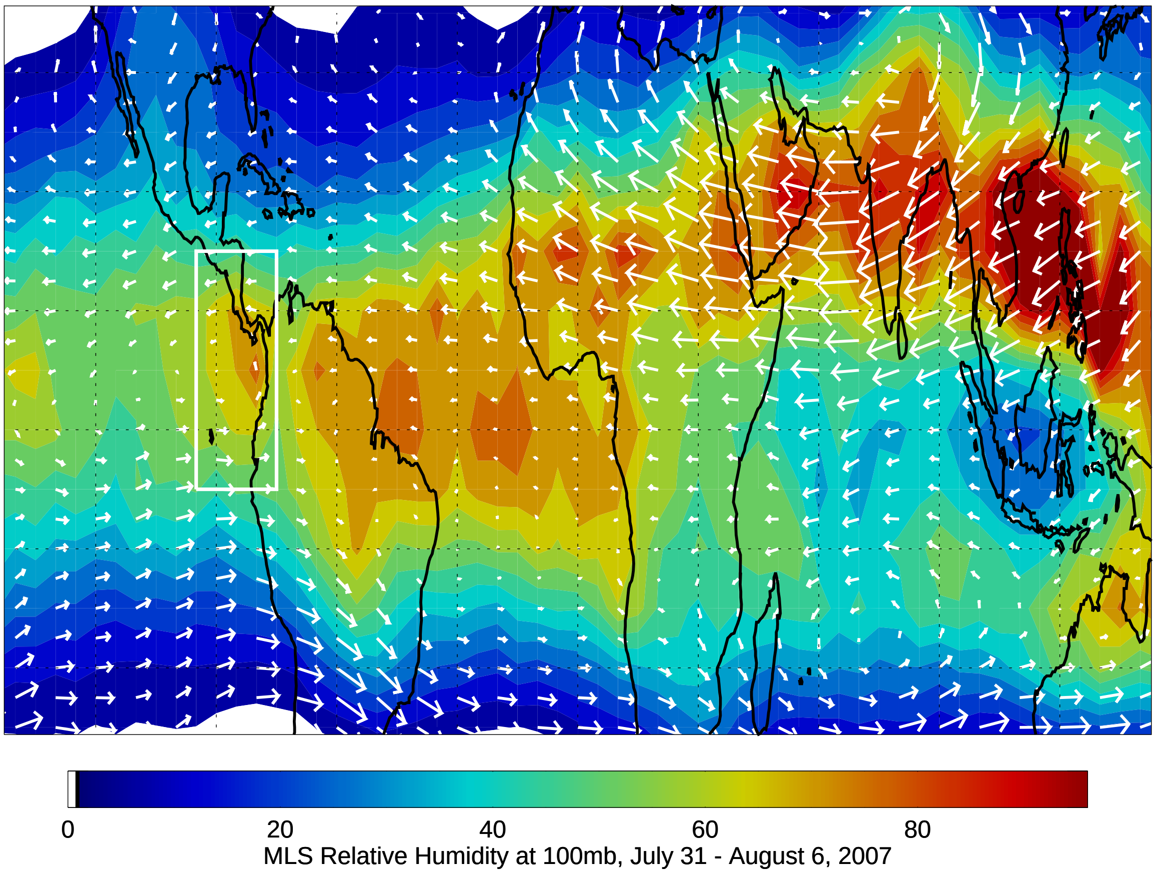

Figure 2. Relative Humidity for a portion of the TC4 period based on MLS measurements and NCEP/NCAR Reanalysis temperatures. Wind vectors indicate the 100mb flow.

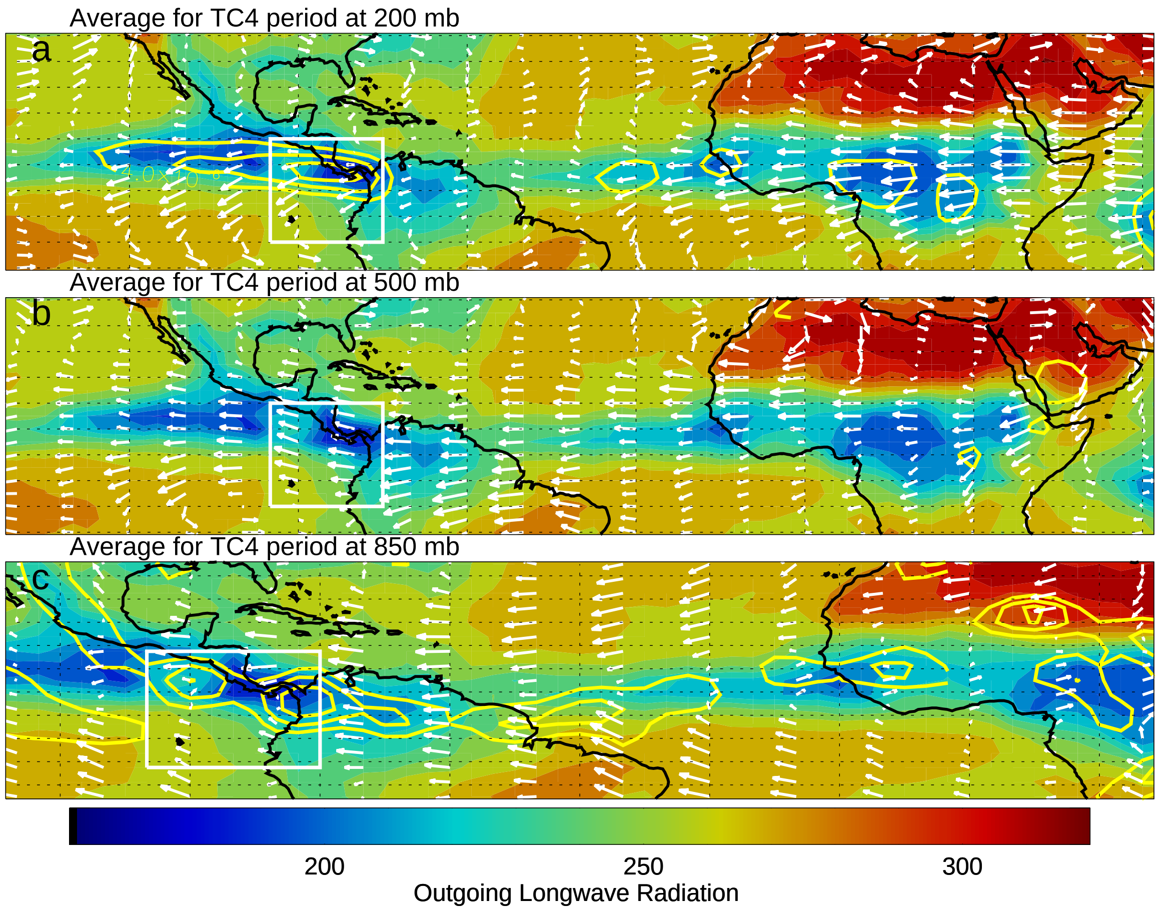

Figure 3. Average meteorology for the TC4 period (July 5 - August 15, 2007) at 200mb (top) 500mb (middle) and 850 mb (bottom). Color fill: OLR; yellow contours: divergence at 200mb and 500mb and convergence at 850mb.

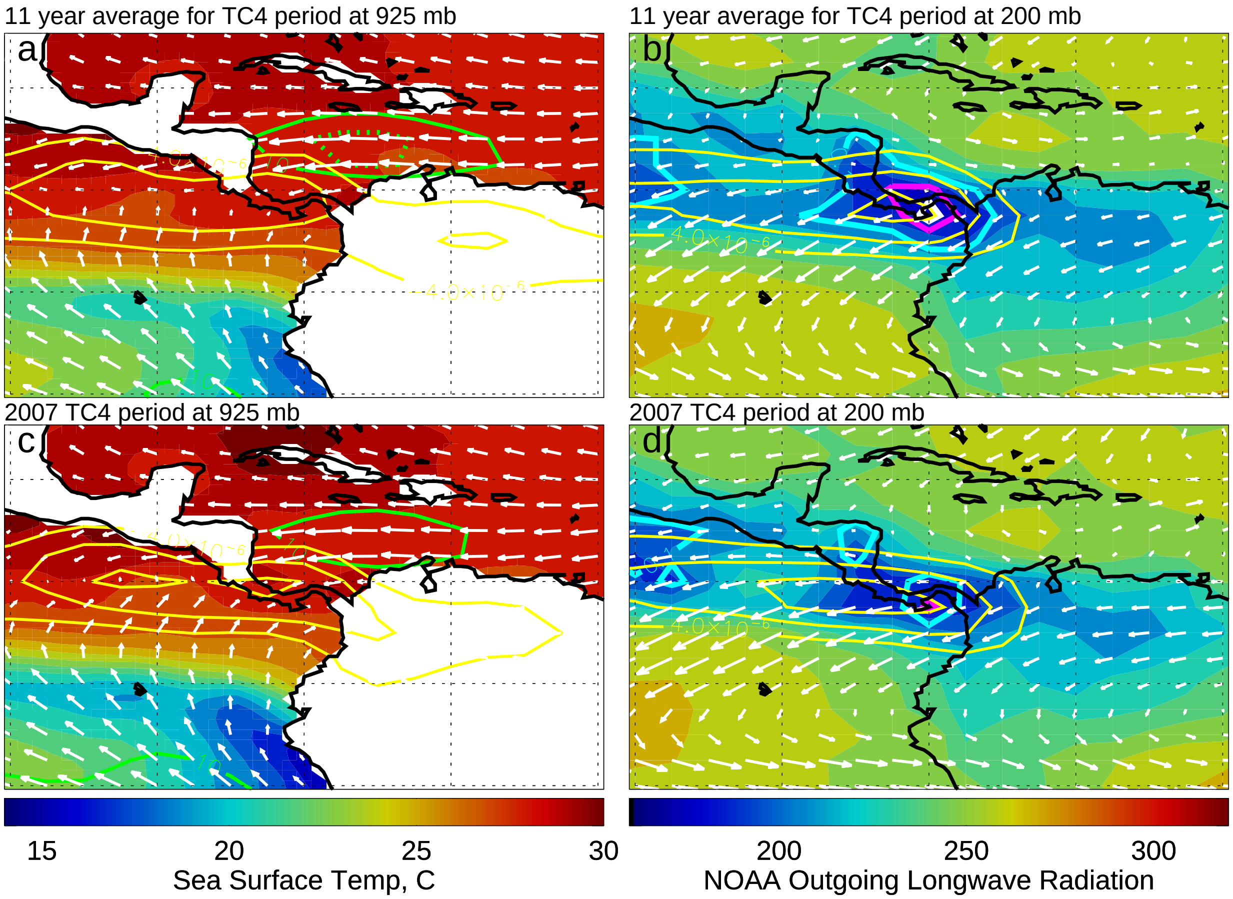

Figure 4. Average meteorology, OLR, and sea surface temperature for the TC4 region. (a) 925mb flow, sea surface temperature (colors), isotachs (green contours)and convergence (yellow contours) for the 11 year average during the TC4 period (July 6 - August 15); (b) 200mb flow, OLR, and divergence (yellow contours) for the 11 year average; (c) as in (a), except for the TC4 period in 2007; (d) as in (b), except for the TC4 period in 2007. See text for description of colored contours in (b) and (d)

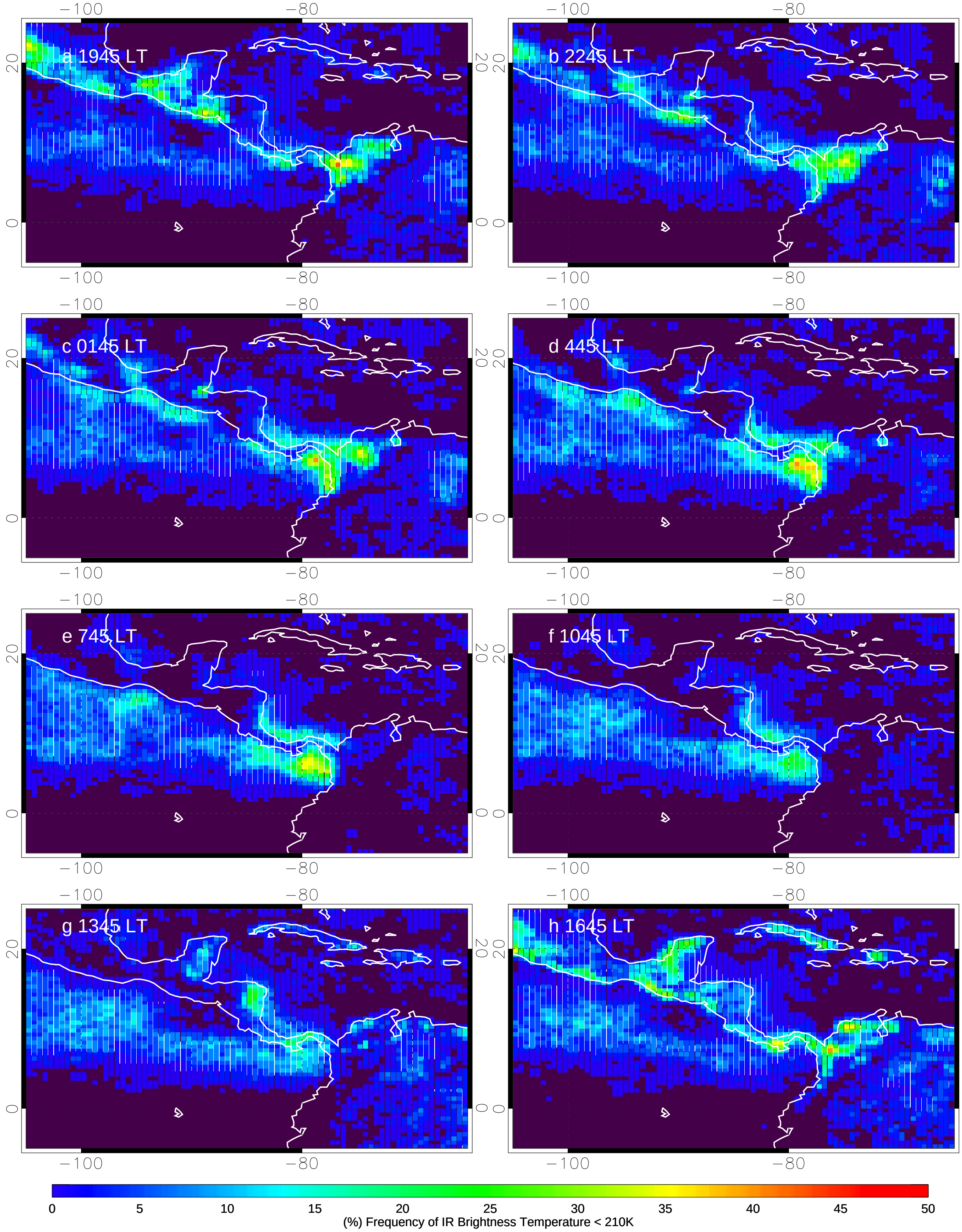

Figure 5. Incidence of cold pixels as a function of local time – see text

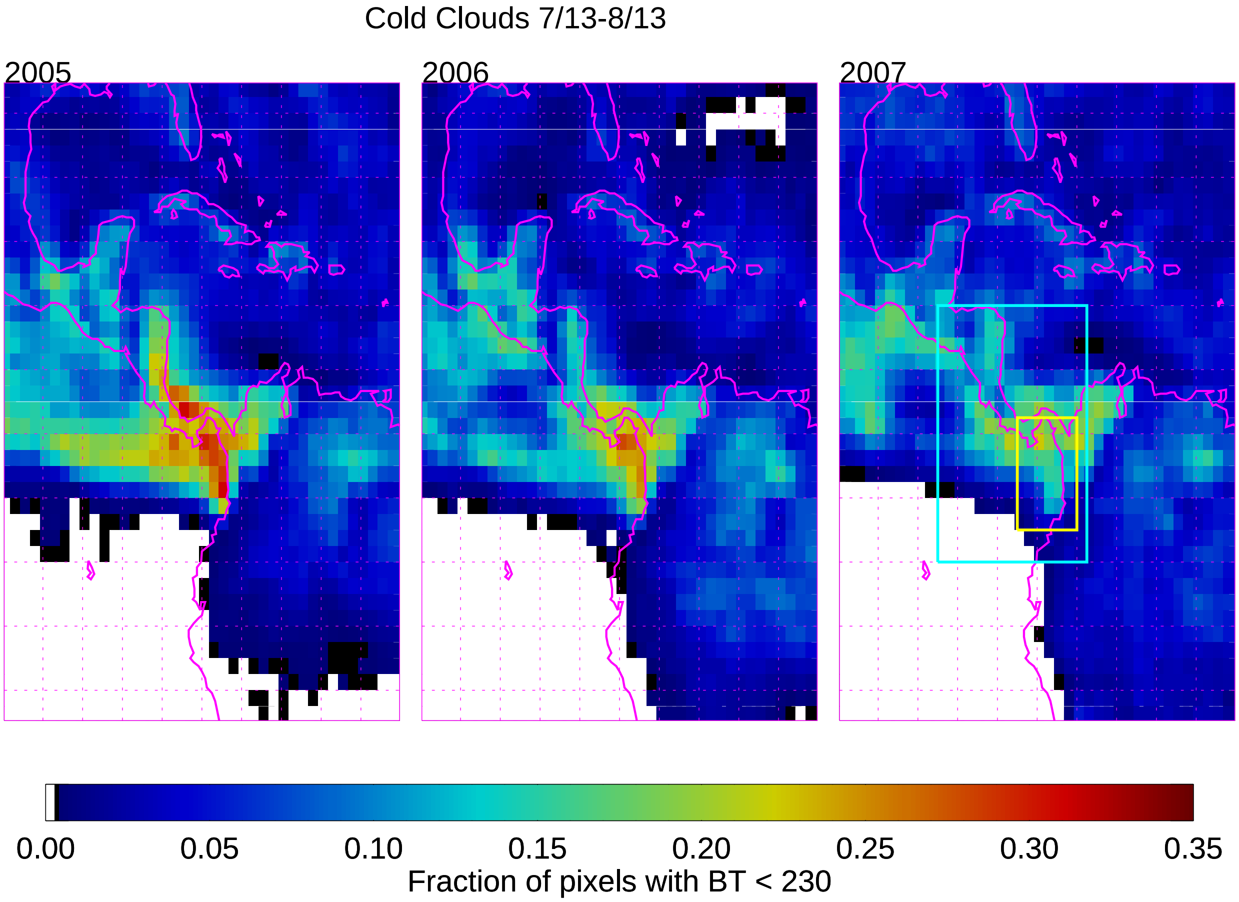

Figure 6. Incidence of pixels with brightness temperatures less than 230K based on GOES-12 imagery for the TC4 period during 2005, 2006, and 2007. The cyan box represents the approximate operating region of the aircraft during TC4. The yellow box represents the Panama Bight region

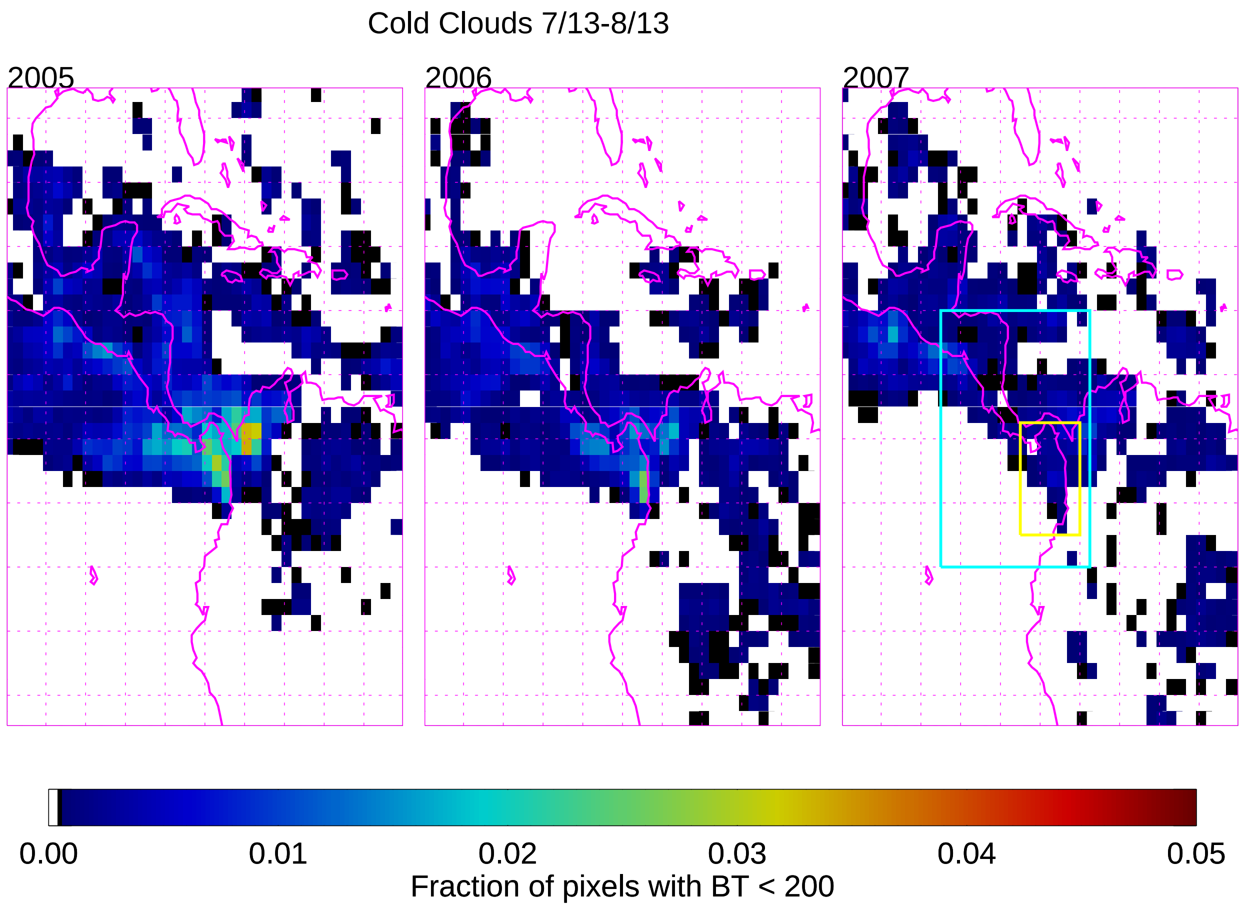

Figure 7. As in Figure 6, escept for brightness temperatures less than 200K.

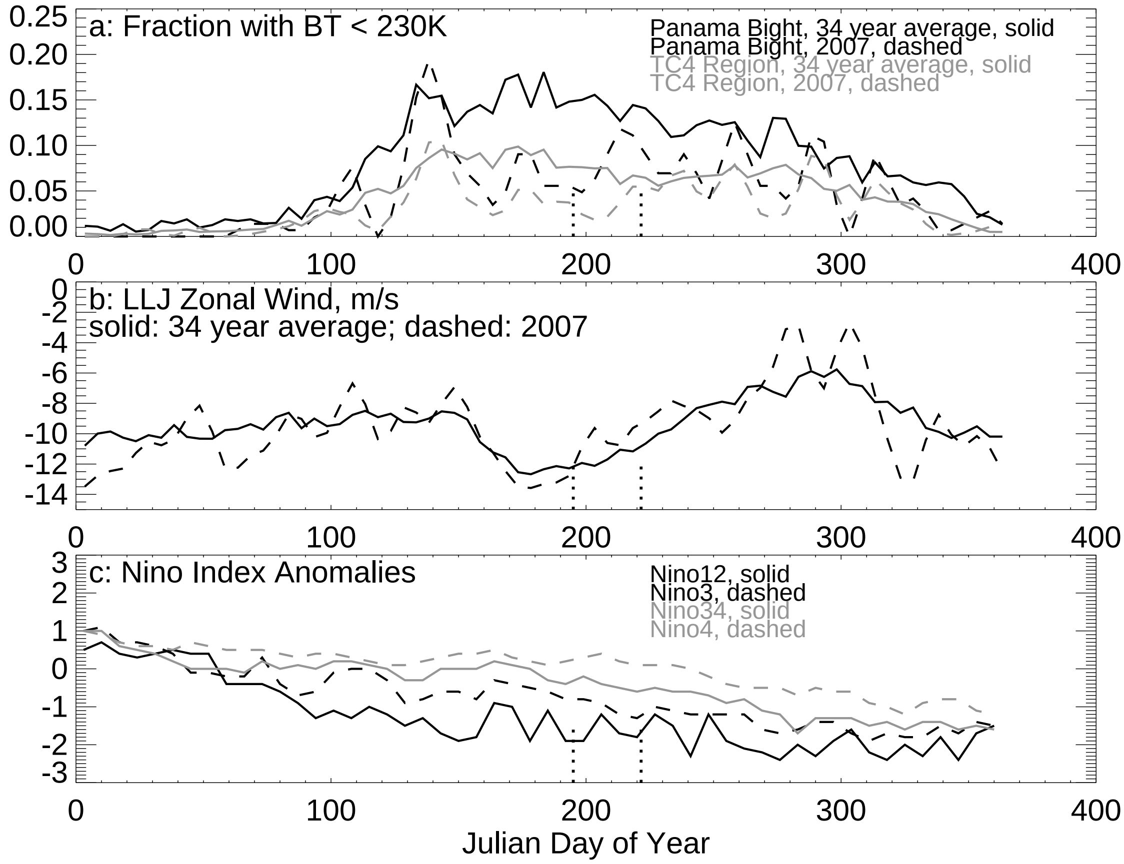

Figure 8. Evolution through the year of convection as shown by OLR (a), the signed strength of the Caribbean Low Level Jet or LLJ (b), and four measures of the Pacific equatorial sea surface temperature anomaly (c). The TC4 experimental period is marked by the vertical dotted lines. See text for details

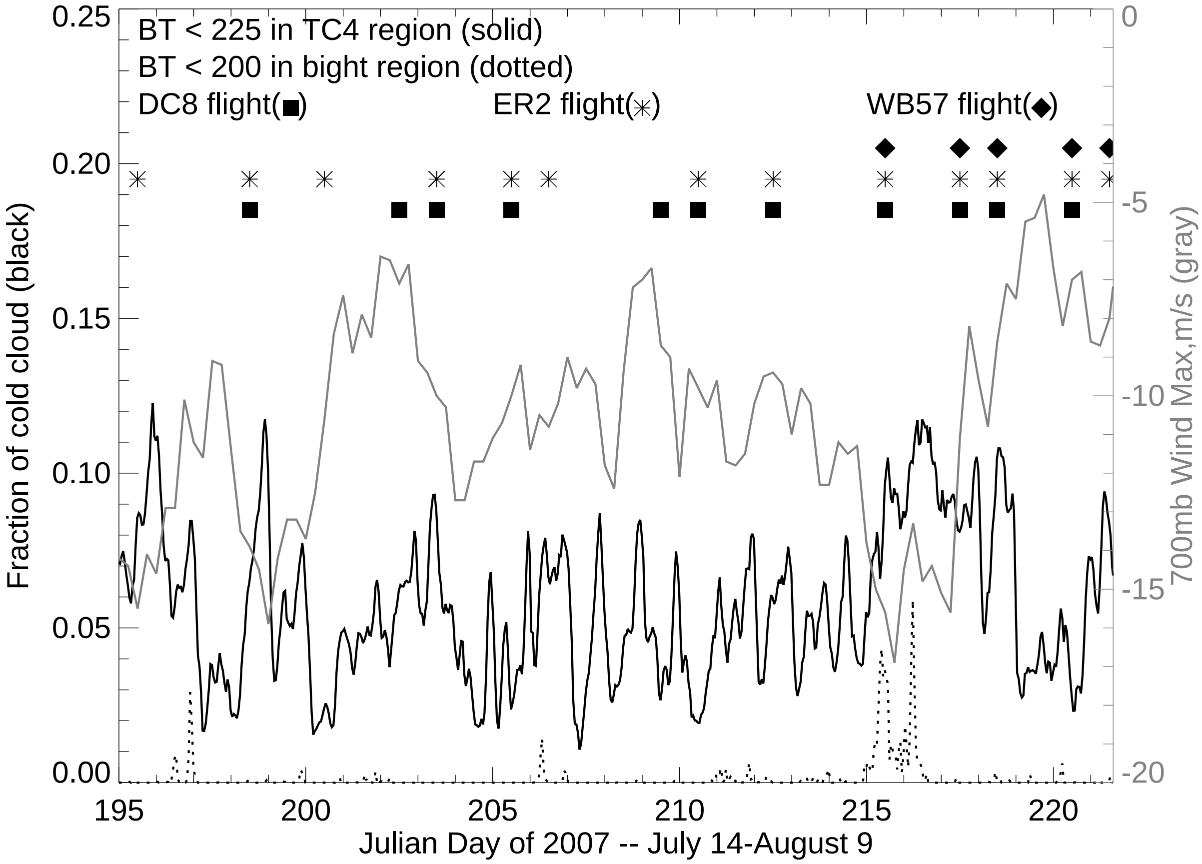

Figure 9. Evolution of convection during TC4, as represented by the fraction of cold cloud using GOES window channel data in the TC4 region (solid black) and the Panama Bight (dotted black), as defined by the yellow and cyan rectangles in Figure 5. The gray line denotes the maximum 700mb wind along the 77.5W meridian from the NCEP/NCAR Reanalysis. The date range is July 14 through August 9, and the dates of the flights by the three aircraft are denoted by indicated symbols. The time axis is Julian day in UTC.

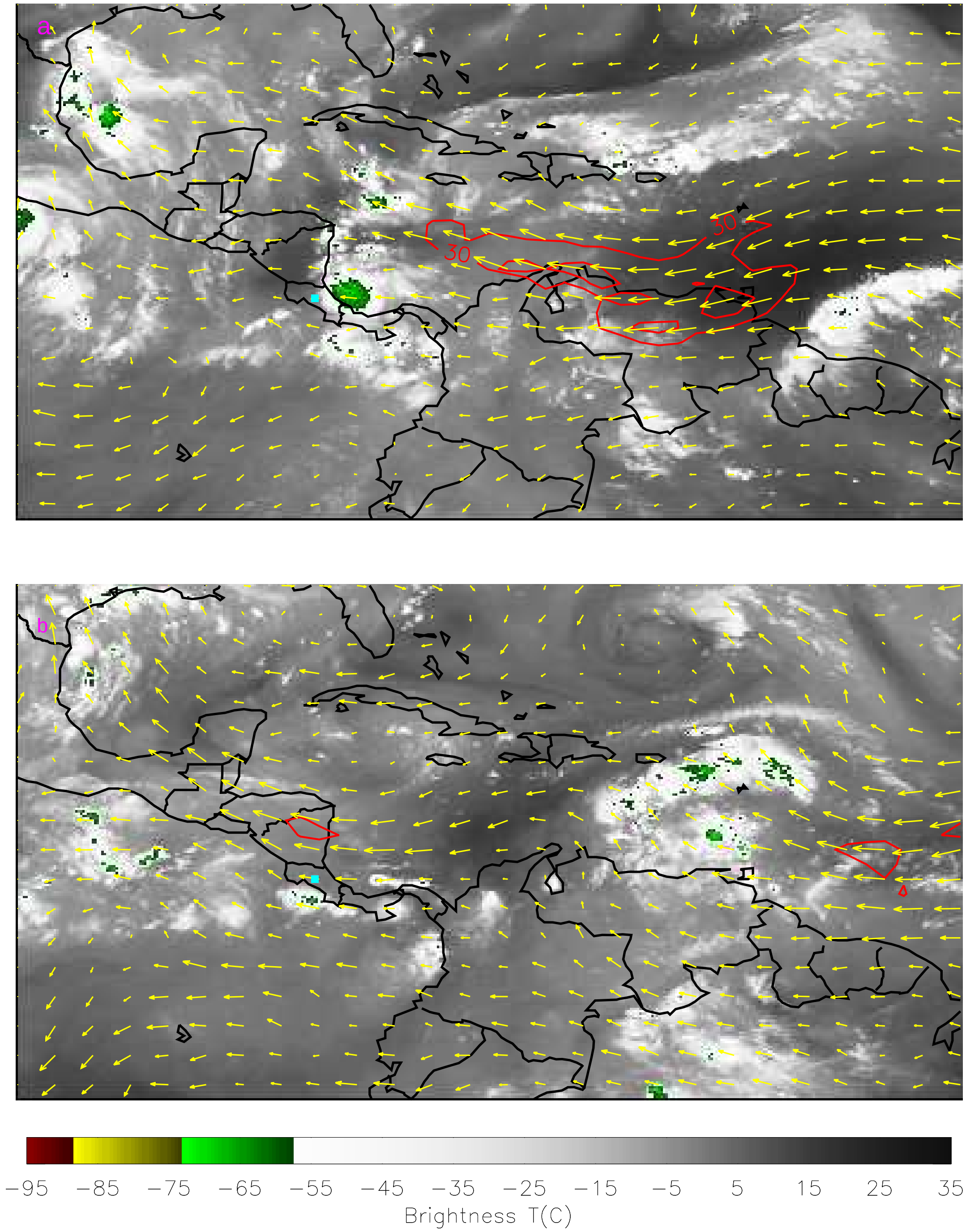

Figure 10. (a) 6.7 μm ("water vapor channel") image for July 17, 2007 at 9 AM local time. Winds are in knots and isotachs above 30 knots are contoured in red. (b) Same as (a), except for July 19, 2007 at 9 AM local time.

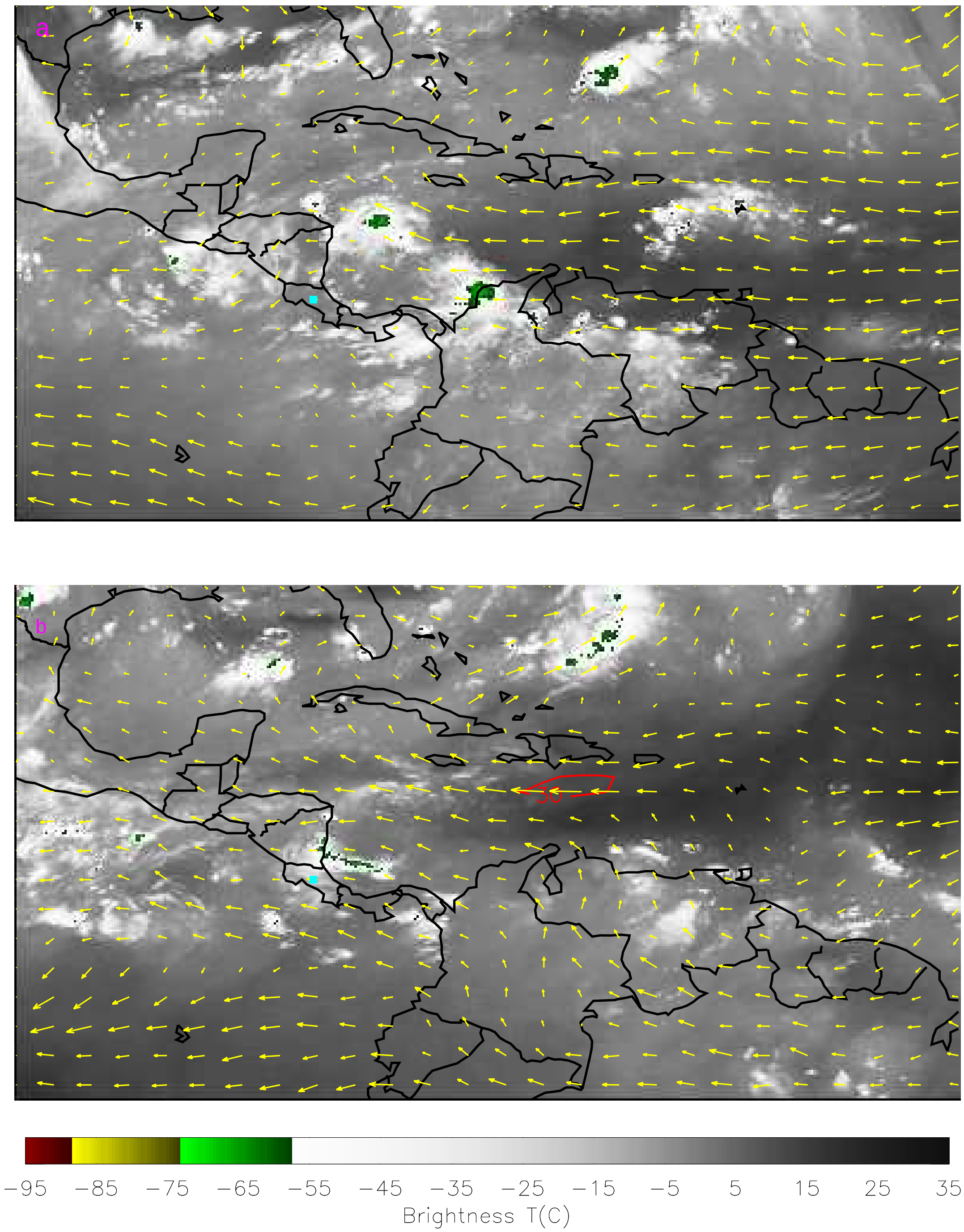

Figure 11. (a) As in Figure 10, except for July 22 at 9 AM local time. (b) As in Figure 10, except for July 29 at 9 AM local time.

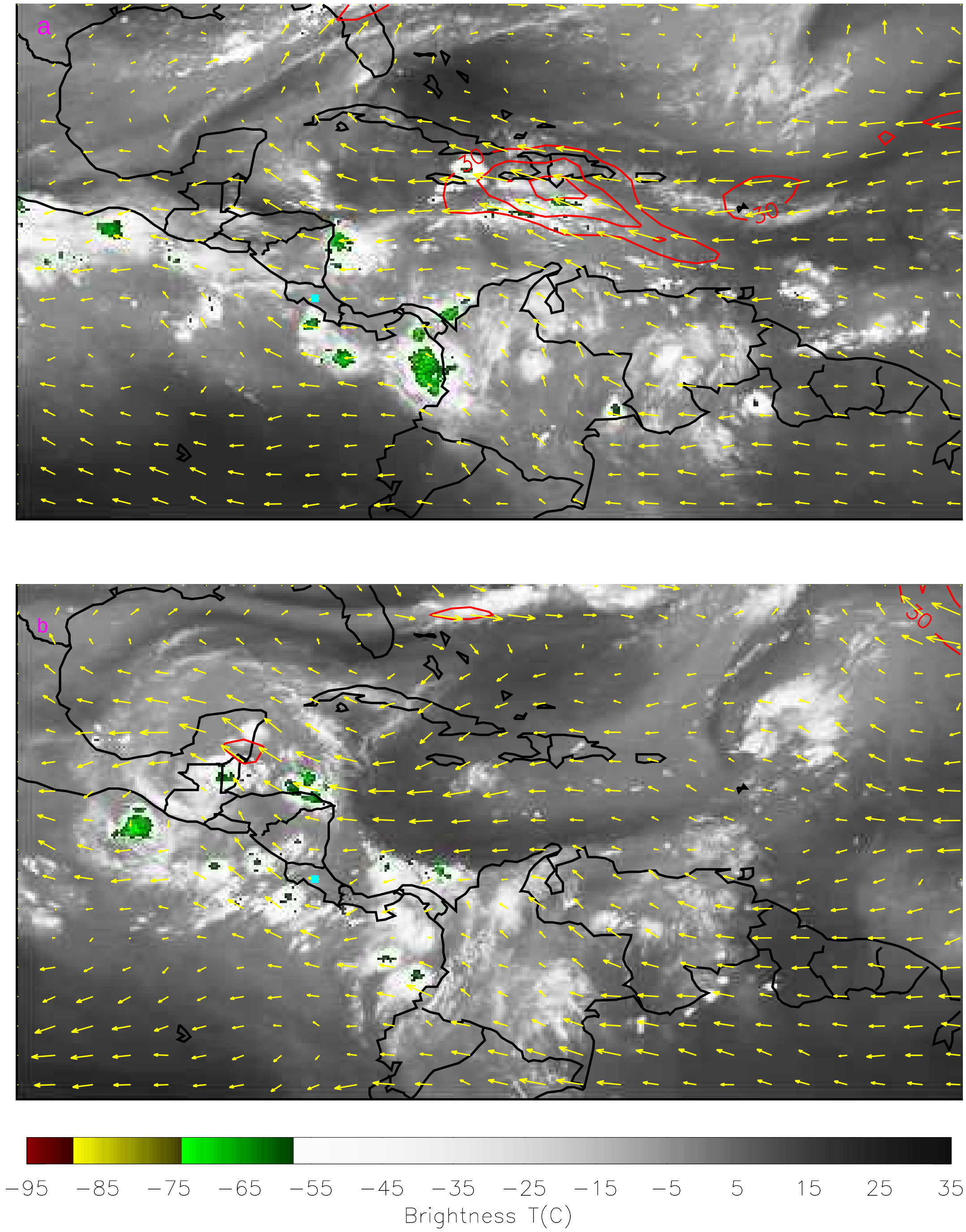

Figure 12. (a) As in Figure 10, except for August 3 at 6 AM local time; (b) As in Figure 10, except for August 5 at 9 AM local time.

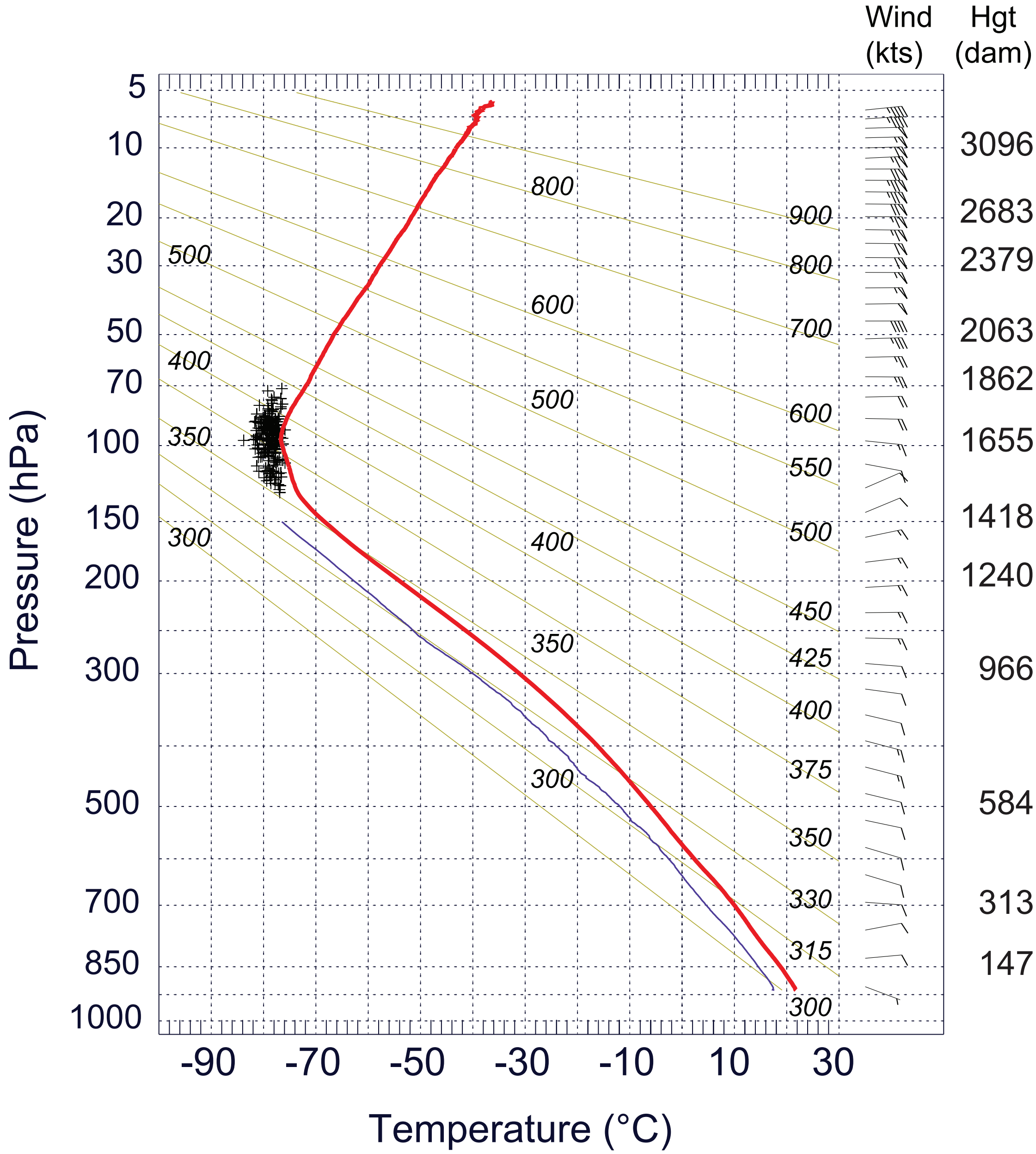

Figure 13. Mean profiles of radiosonde temperature (T), dewpoint (Td) and winds at Alajuela, Costa Rica (10.0°N, 84.2°W), 16 June - 15 August, 2007. Crosses are cold point tropopauses from individual soundings. Mean geopotential height (dam) on standard levels at right. Isentropes labeled from 300 to 900 K.

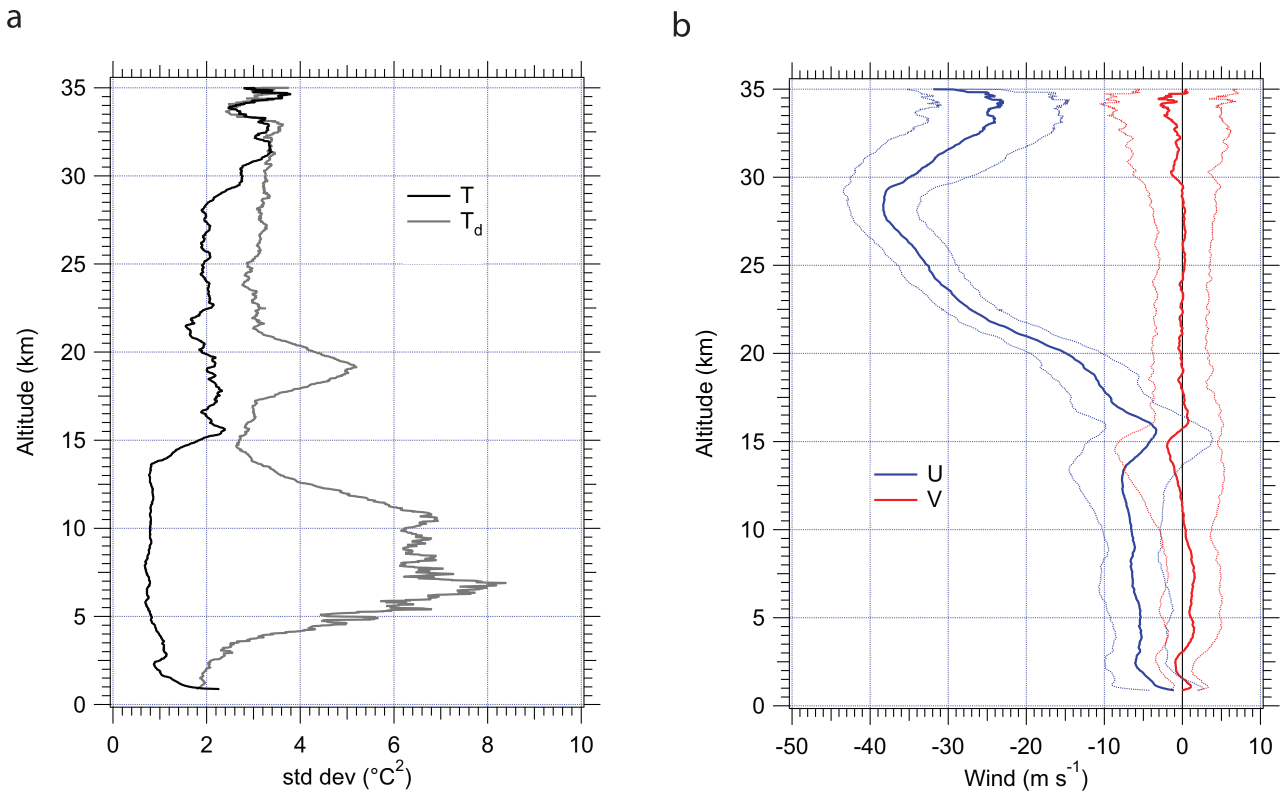

Figure 14. (a) Standard deviation of (a) temperature and dewpoint and (b) average zonal (u) and meridional (v) winds at Alajuela, Costa Rica in envelopes of ±1 standard deviation. Data as in Figure 13.

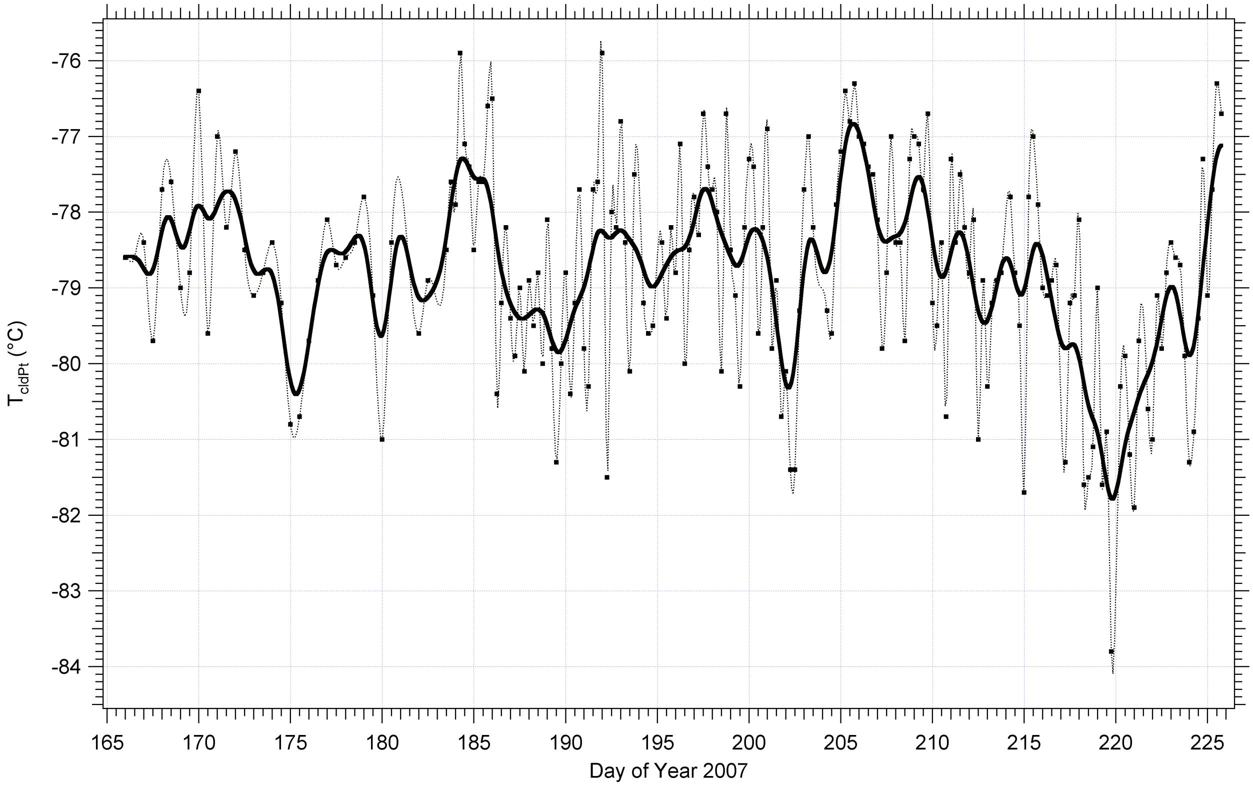

Figure 15. Time series of cold point tropopause temperature, 16 June 00 UT through 15 August 18 UT (day 166-226.75) from radiosondes at Alajuela, Costa Rica. Dots are observations, thin dotted lines are a series generated with cubic-spline interpolation and the heavy black line is the latter smoothed with a 53-pt binomial smoother.

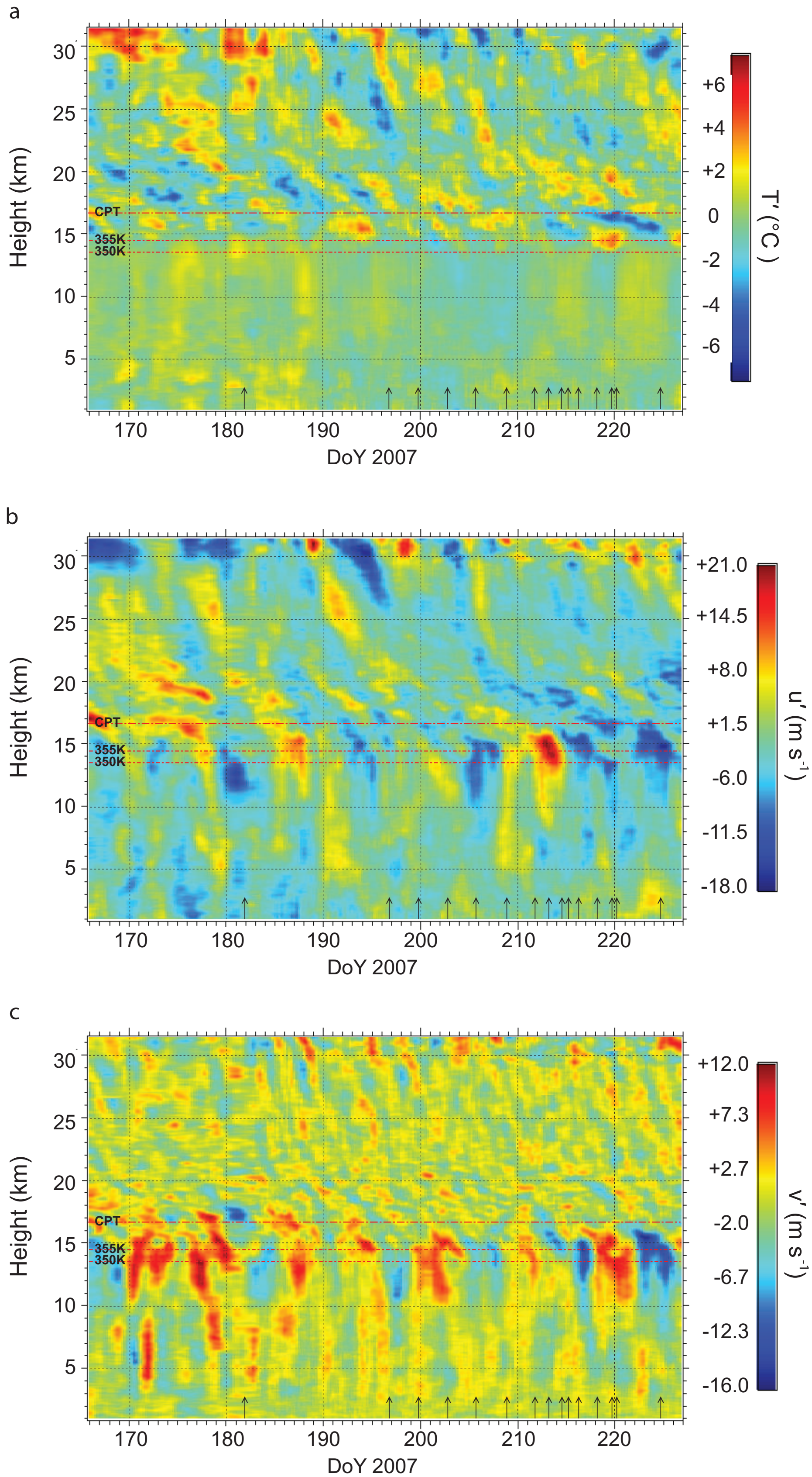

Figure 16. Time-height cross-sections of anomalies of (a) temperature, (b) zonal wind and (c) meridional wind at Alajuela, Costa Rica, 16 June - 14 August 2007. Red horizontal dashed lines at mean altitudes of the 350K and 355K potential temperature surfaces and the cold point tropopause. Vertical arrows at the times of flights of the CFH/ECC payloads.

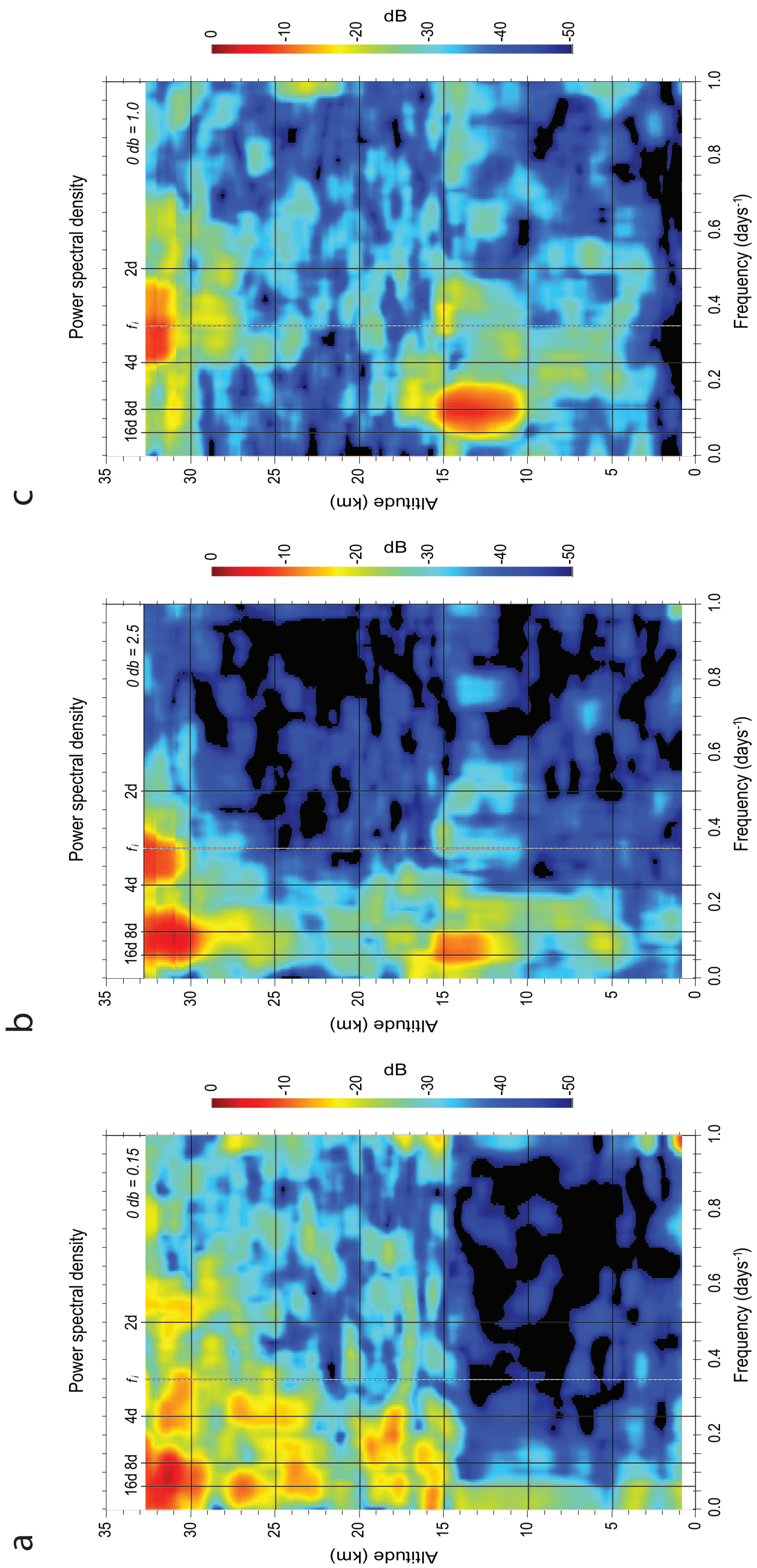

Figure 17. Frequency-height cross-section of power spectral density from periodogram analyses of anomalies at Alajuela, Costa Rica, 16 June - 15 August 2007, of (a) temperature, (b) zonal wind and (c) meridional wind.

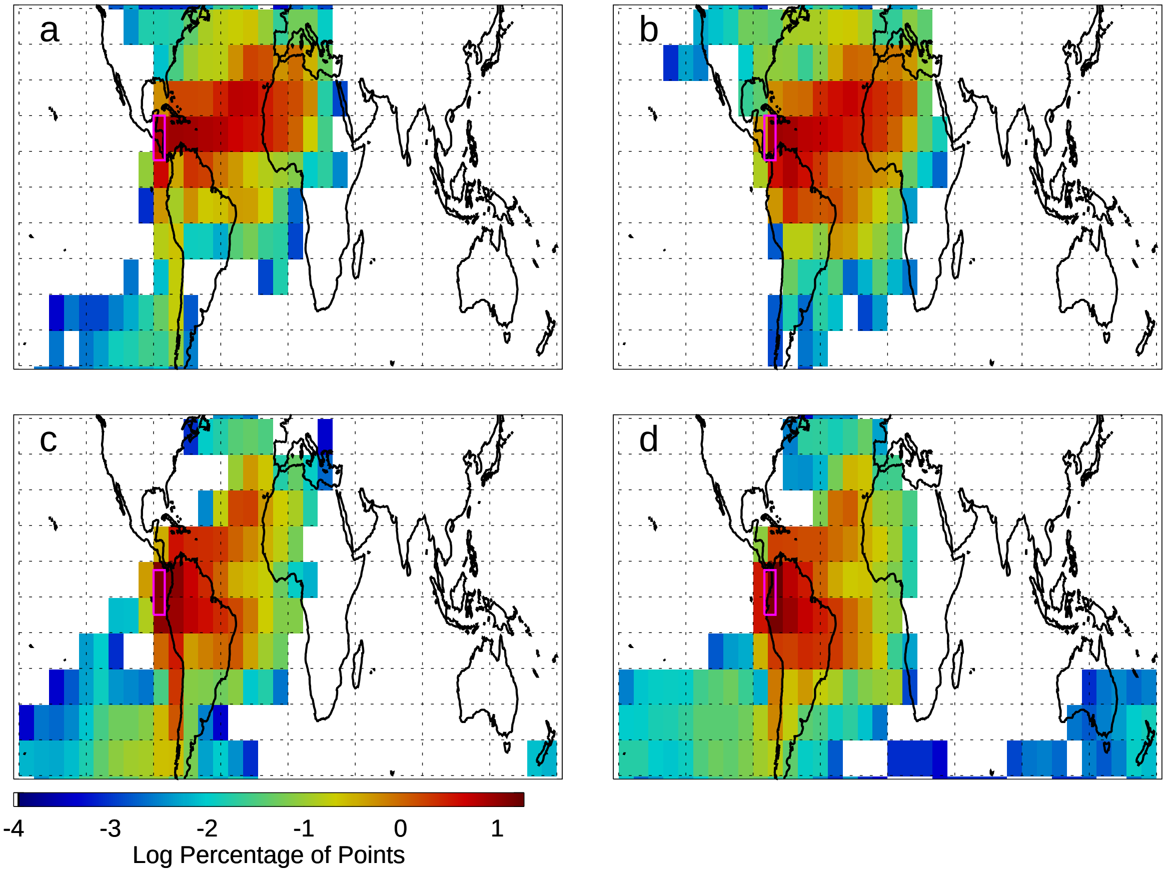

Figure 18. Geographical percentage distribution function from back trajectories originating at 850mb in four quadrants in the TC4 region. Trajectories originate between: (a) 7.5N and 20N, and 90W and 82.5W; (b) 7.5N and 20N, and 82.5W and 75W; (c) 5S and 7.5N and 90W and 82.5W; (d) 5S and 7.5N and 82.5W and 75W. The magenta rectangles outline each of the four quadrants.

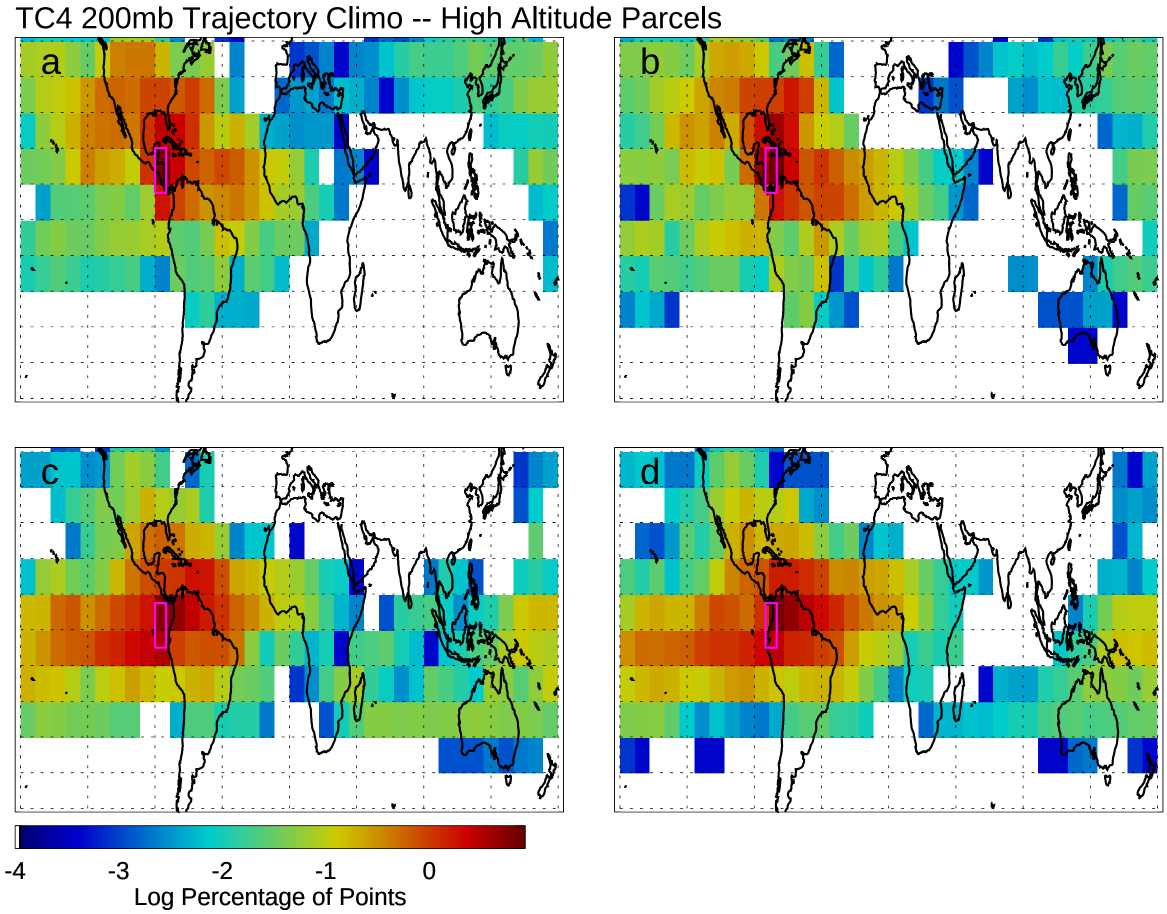

Figure 19. As in Figure 18 except for trajectories originating at 200mb with points remaining above 300mb

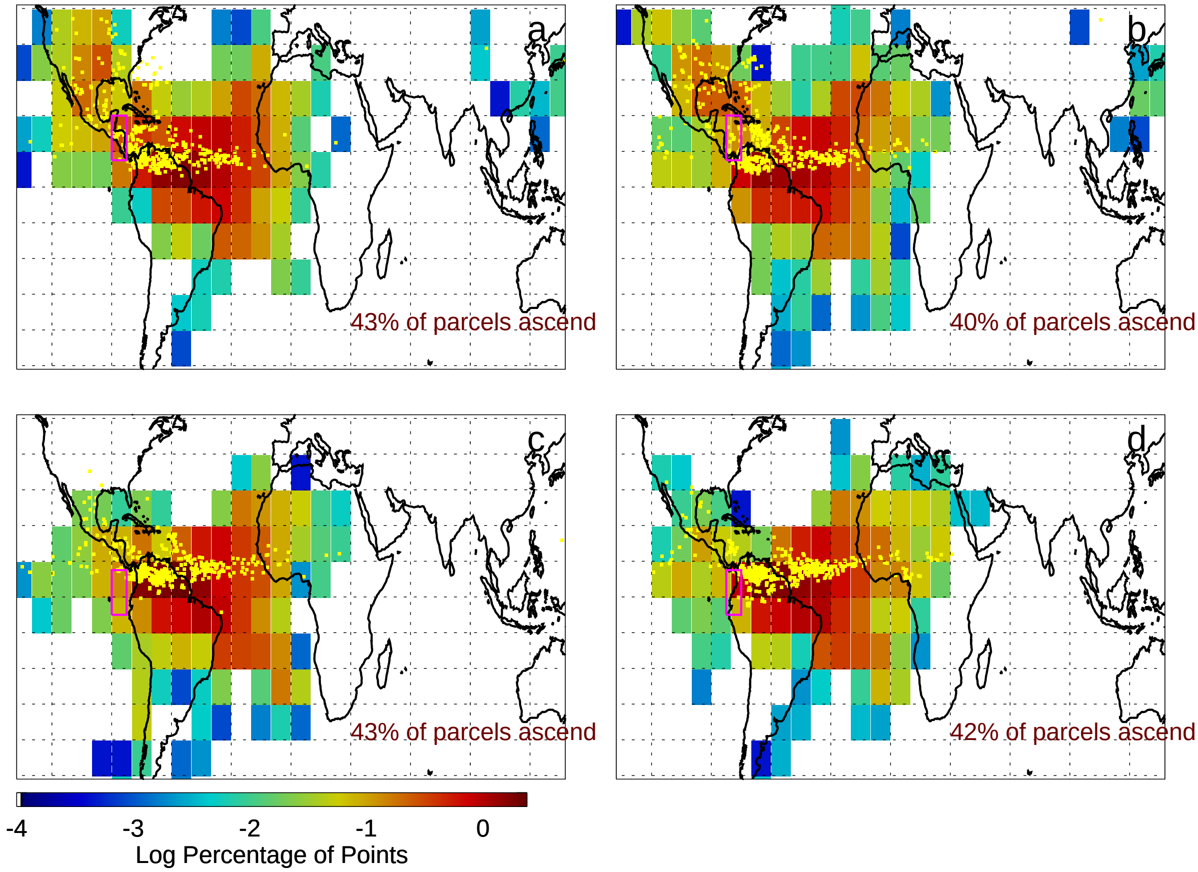

Figure 20. Distribution of points located below 700mb on back trajectories that originate at 200mb. a-d represent results for quadrants as defined in Figure 18. See text.

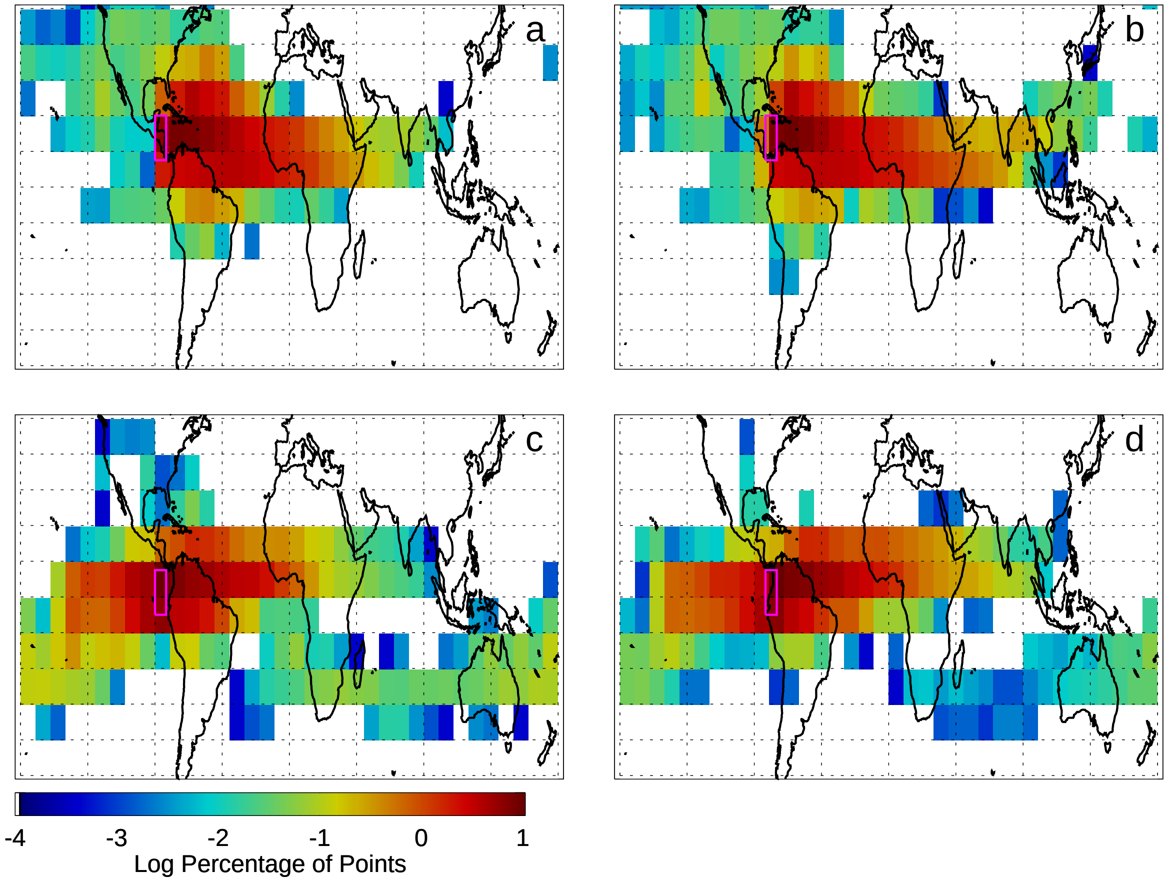

Figure 21. As in Figure 19, except for trajectories originating at 100mb and points above 200mb.

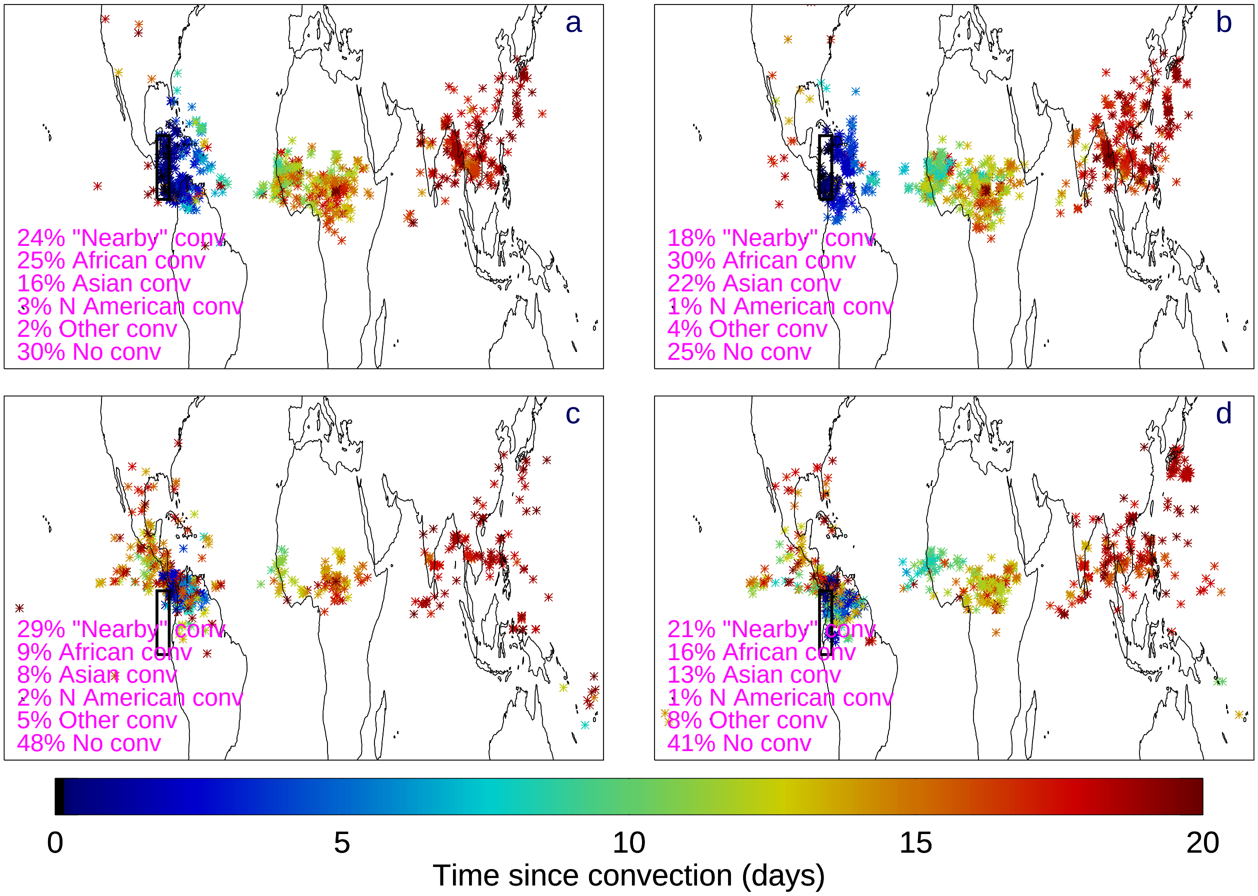

Figure 22. Distribution of points located below 700mb on back trajectories that originate at 200mb. a-d represent results for quadrants as defined in Figure 18.